

# Nanoscale Advances

Accepted Manuscript

This article can be cited before page numbers have been issued, to do this please use: X. Yang, J. Shu, Z. Zhou and H. Liang, *Nanoscale Adv.*, 2024, DOI: 10.1039/D4NA00292J.



This is an Accepted Manuscript, which has been through the Royal Society of Chemistry peer review process and has been accepted for publication.

Accepted Manuscripts are published online shortly after acceptance, before technical editing, formatting and proof reading. Using this free service, authors can make their results available to the community, in citable form, before we publish the edited article. We will replace this Accepted Manuscript with the edited and formatted Advance Article as soon as it is available.

You can find more information about Accepted Manuscripts in the [Information for Authors](#).

Please note that technical editing may introduce minor changes to the text and/or graphics, which may alter content. The journal's standard [Terms & Conditions](#) and the [Ethical guidelines](#) still apply. In no event shall the Royal Society of Chemistry be held responsible for any errors or omissions in this Accepted Manuscript or any consequences arising from the use of any information it contains.

### Declaration of interests

The authors declare that they have no known competing financial interests or personal relationships that could have appeared to influence the work reported in this paper.

The authors declare the following financial interests/personal relationships which may be considered as potential competing interests:



## Polyimide as a biomedical material: advantages and applications

View Article Online

DOI: 10.1039/D4NA00292J

Junjie Shu <sup>1</sup>, Zhongfu Zhou <sup>2</sup>, Huaping Liang <sup>1\*</sup> and Xia Yang <sup>1\*</sup>

<sup>1</sup> Department of Wound Infection and Drug, State Key Laboratory of Trauma and Chemical Poisoning, Daping Hospital, Army Medical University (Third Military Medical University), Chongqing, China

<sup>2</sup> Inner Mongolia Key Laboratory of New Carbon Materials, Baotou, China

\*Corresponding authors. E-mail addresses: 13638356728@163.com (H. Liang), oceanyx@126.com (X. Yang).



**Abstract**

1 As a class of polymers, polyimides (PIs) are characterized by strong  
2 covalent bonds, which have the advantages of high thermal weight, low  
3 weight, good electronic properties and superior mechanical properties.  
4 They have been successfully used in the fields of microelectronics,  
5 aerospace engineering, nanomaterials, lasers, energy storage and painting.  
6 Its biomedical application has attracted extensive attention, and it has  
7 been explored for its use as an implantable, detectable, and antibacterial  
8 material in recent years. This article summarizes the progress of PI in  
9 terms of three aspects: synthesis, properties, and application. First, the  
10 synthetic strategies for PI are summarized. Then, the properties of PI as a  
11 biological or medical material are analyzed. Finally, the applications of PI  
12 in electrodes, biosensors, drug delivery systems, bone tissue replacements,  
13 face masks or respirators, and antibacterial materials are introduced. The  
14 present review provides a comprehensive understanding of the newest  
15 progress of the PI, thereby providing a basis for developing new  
16 potentially promising materials for medical applications.

**Keywords:** polyimide; synthesis; characters; properties; medical application.



## 1. Introduction

17 After decades of research in materials science and tissue engineering, the  
18 capacity to create functional human tissue models for the whole repair of  
19 organ functions *in vivo* and *in vitro* is still challenging. A large number of  
20 materials and technologies have been constructed, investigated, and  
21 manufactured, but only a few have been successfully applied in the clinic.  
22 To achieve successful translation of medical materials into clinical  
23 practice, the ideal characteristics of these materials include the ability to  
24 mimic native organ structure and function, no toxicity, perfect integration  
25 into and interaction with tissues, and adaptation of the morphology and  
26 function of the organism, including sufficient vascular supply, no  
27 thrombus and active response to challenging environments such as cancer,  
28 inflammation, and infection<sup>1</sup>. Therefore, an increasing number of  
29 investigations focusing on medical materials have been designed due to  
30 some directional improvements that could rescue the functions of organs  
31 and tissues.

32 Currently, successful examples of applications of medical materials such  
33 as intraocular lenses<sup>2</sup>, poly(4-methyl-1-pentene) (PMP) artificial lung  
34 membranes for extracorporeal membrane oxygenation (ECMO)<sup>3</sup>, and  
35 filtration membranes for continuous renal replacement therapies (CRRTs)<sup>4</sup>  
36 have provided groundbreaking solutions to the choke points in related  
37 fields with the rapid development of medical devices, and the demands of  
38 some of these medical-related materials are considerable. For example,  
39 there are more than 7-20 million lens implant candidates annually  
40 worldwide<sup>5</sup>. The cost of ECMO therapy support for surviving adult  
41 patients diagnosed with acute respiratory distress syndrome is high, at  
42 approximately \$98,784,116<sup>6</sup>. A total of 68% of 100,000 ECMO survivors  
43 are treated at more than 300 centers worldwide <sup>6</sup>, and ECMO has been  
44 proven to be an effective approach for saving the lives of these patients.  
45 The global market demand for hemostatic material was valued at USD



46 20.8 billion in 2022 and is predicted to progressively increase at a  
47 compound annual growth rate of 5.4% from 2022 to 2027<sup>7</sup>. This situation  
48 worldwide encourages academics as well as the pharmaceutical and  
49 medical dressing or equipment industries to investigate more new products  
50 for the treatment of these diseases. However, in some cases, the properties  
51 of these materials cannot meet clinical expectations under complex  
52 pathological conditions *in vivo*. For example, artificial blood vessels that  
53 can be long-term implanted in the body without adverse reactions such as  
54 thrombosis caused by lower limb ischemia are lacking<sup>8</sup>. The oxidized  
55 cellulose-based commercial hemostatic material Surgicel® is highly  
56 effective in blocking small arterial bleeding and reducing intracranial  
57 hematoma in bleeding patients. However, the acidic microenvironment can  
58 potentially induce an inflammatory response, delaying the wound-healing  
59 process and damaging peripheral nerves<sup>9</sup>. How can we improve the  
60 functions and overcome the shortcomings of these materials? One  
61 effective way is to develop composite materials, which is a new hope for  
62 expanding the range of single biomaterial applications in the medical  
63 field. For example, chitosan combined with quaternary ammonium groups  
64 improved the antibacterial properties of this special material<sup>10</sup>. Another  
65 way is continuing to innovate the existing medical material and  
66 technology, and the materials become increasingly complicated and  
67 diversified; the performance of these newer medical materials could  
68 satisfy the demands with no additional adverse reactions.

69 Notably, numerous studies have shown that polyimide (PI) has excellent  
70 physical and chemical properties, including low weight, flame  
71 retardancy, high-temperature resistance, low-temperature tolerance,  
72 excellent mechanical properties, chemical solvent and radiation resistance,  
73 flexibility, and good dielectric properties<sup>11</sup>. It has been concluded that PI  
74 has been proven to be an important industry material for military armor,  
75 aerospace areas, radomes, liquid crystal alignments, microelectronics,



76 solar-to-electrochemical energy storage, photocatalysis, electrocatalysis  
77 applications, etc.<sup>12</sup>. PIs are now widely used as membranes for the  
78 insulation of solar cell base plates and motor slots, for separating  
79 membranes in permeation vaporization and ultrafiltration, for repairing  
80 enameled wire, for insulating fibres in high-temperature media and  
81 bulletproof and fireproof fabrics, for adhesives in high-temperature  
82 structural adhesives, for photoresists in color filter films, for  
83 microelectronics in dielectric layers and protective layers, for liquid  
84 crystal displays in orientation agent materials, for electro-optical  
85 materials in optical switch fields and composites in aviation and aerospace  
86 fields<sup>13, 14</sup>. Additionally, advanced healthcare PIs were designed to include  
87 puncture needle-type devices, artificial hip joints, microelectrode arrays  
88 for nerve stimulation<sup>15</sup>, drug delivery<sup>16, 17</sup>, biosensors<sup>18</sup>, and other aspects  
89 of medical utilization<sup>19, 20</sup>. Therefore, several recent studies have  
90 described the design of PIs for medical material applications, including  
91 resins, powders, films, fibers, foams, and soluble PIs (Fig. 1). We aim to  
92 review the relevant literature on the synthesis and structural  
93 characteristics, properties, and application of PI as a medical material and  
94 its trends and outlook in the present review.

## 95 **2. Synthesis of PI**

96 PIs with cyclic aliphatic, hetero, chiral, fluorinated, carbazole, nonlinear  
97 optical, nanometer-sized and unsymmetrical structures are derived from  
98 noncoplanar monomers (kink, spiro, and cardo structures). PIs can be  
99 divided into aliphatic and aromatic polyimides according to their chemical  
100 composition. Aromatic PIs are commonly synthesized from the  
101 polycondensation of various monomers, including diamine and  
102 dianhydride, which are composed of a sequence of aromatic groups with  
103 imide linkages (-CO-N-CO-)<sup>21</sup>. PI fibers were initially carried out by  
104 Americans as early as the 1960s and then investigated by Japanese, Soviet,  
105 French, Austrian, and Chinese investigators<sup>22</sup>.



## 106 **2.1 Typical synthesis process**

107 The typical synthesis process of PI involves the loading of crystalline  
108 benzoic acid (BA) (9.0 g) and phthalic anhydride (PA) (0.7287 g) into a  
109 glass reactor equipped with a heater, stirrer, and an inert gas inlet. With  
110 the gas in the reactor at 140°C, 3,4'-ODA (0.2803 g) was added to the  
111 mixture. The reaction mixture was stirred at 150°C for 2 h, accompanied  
112 by the slow addition of inert gas. Then, this hot liquid reaction mixture  
113 was transferred to a glass container and cooled to room temperature. Next,  
114 the solidified reaction mixture was extracted and washed repeatedly with  
115 acetone or diethyl ether to remove the excess BA. Finally, the reaction  
116 product of the polymer was filtered and dried under vacuum, and PI  
117 powder was obtained. One improved method reported that PI was also  
118 obtained in 99% yield within 1 h from a polyamic acid intermediate using  
119 the "beat and heat" method, which included solvent-free vibrational ball  
120 milling and a thermal treatment step<sup>23</sup>. After the PI powder was obtained,  
121 it was hot pressed at 300~380°C or from a 2% solution in chloroform to  
122 form PI films (Fig. 2A)<sup>24</sup>. This study presented a straightforward route to  
123 synthesize PI powders and films.

## 124 **2.2 Dry- and wet-spinning methods**

125 Some studies have reported that PI fibers are mostly synthesized by dry-  
126 spinning and wet-spinning methods. In the wet-spinning method, organic-  
127 soluble PI or polyamic acid (PAA) solutions are forced into a nonsolvent  
128 fluid to separate the fibres from the solvent. Then, the generated fibers are  
129 annealed under tension to remold the tensile strength and modulus.  
130 Compared with the wet-spinning method, organic solvents are evaporated  
131 directly from extruded PAA fibers at high temperatures, and a partial  
132 imidization reaction occurs in a mixture of hot gases during the dry-  
133 spinning process (Fig. 2B)<sup>22</sup>. The spinning speed is increased to improve  
134 the production of PI fibers by the dry-spinning process. The quality of PI  
135 fibers is better when using wet-spinning or dry-wet-spinning methods.





### 136 **2.3 One-step and two-step processes**

137 In addition, according to the main difference between spinning solutions  
138 and reaction mechanisms, two main strategies, defined as one-step and  
139 two-step processes, are also used to prepare PI fibers. In a one-step  
140 method, PI fibers are produced directly from highly boiling organic-  
141 soluble PI solutions at 180-220°C to undergo a rapid imidization reaction.  
142 In the two-step method, PAA solutions are obtained first after reacting  
143 dianhydride and diamine monomers in dipolar aprotic solvents and then  
144 converted into final PI fibers through thermal or chemical imidization  
145 (Fig. 2C)<sup>25</sup>. P-phenylenediamine (PDA) and 3,3',4,4'-biphenyltetra-  
146 carboxylic dianhydride (BPDA) are combined to obtain precursor fibers of  
147 PAA via a dry-jet wet-spinning process. Subsequently, the PAA fibers  
148 were heated from room temperature to 300, 350, and 400°C to form PI  
149 fibers, and the tensile modulus of the PI fibers was highly dependent on  
150 the heating rate<sup>25</sup>. In addition, PAA can also be obtained from the reaction  
151 of 4,4'-oxydianiline (4,4'-ODA) (3.97 g) and pyromellitic dianhydride  
152 (PMDA) (4.33 g) in 35 ml of N,N-dimethylformamide (DMF) by  
153 polycondensing with stirring for 8 h. The PAA solution was electrospun at  
154 15 kV 15 cm from the needle to the collector and then subjected to  
155 thermal imidization (Fig. 2D)<sup>26</sup>. Finally, PI nanofibers were prepared.

### 156 **2.4 Thermoplastic or thermosetting methods**

157 According to their processing characteristics, PI fibers can also be  
158 classified as thermoplastic or thermosetting. The thermoplastic partially  
159 crystalline PI powder was distributed on continuous carbon fibers via  
160 electrostatic spraying, and further hot calendaring and pressing were  
161 applied. The obtained carbon plastics lead to a rise in glass transition and  
162 thermal decomposition temperatures up to 590°C due to being composited  
163 with PI (Fig. 2E)<sup>27</sup>. The physical properties of thermosetting PI include a  
164 higher glass transition temperature and storage modulus and better shape  
165 fixity than thermoplastic PI due to low-density covalent crosslinking (Fig.



166 2F)<sup>28</sup>. Hyperbranched PI was prepared to modify bismaleimide (BMI)  
167 resin to achieve higher impact strength (Fig. 2G)<sup>29</sup>. Based on the use of  
168 chemical or physical crosslinking reactions, thermoplastic or  
169 thermosetting processes are chosen.

## 170 **2.5 The modified synthesis process**

171 Moreover, other investigations have investigated the imidization process,  
172 evaporation, chain orientation, crystallization, subprocesses of solvents,  
173 chemical conversion, and composition to improve the properties of PI  
174 materials<sup>25</sup>. The PIs synthesized from symmetric 4,4'-oxydianiline (4,4'-  
175 ODA) are amorphous and have a low glass transition temperature (Fig.  
176 2H)<sup>30</sup>. The introduction of 2,4,5,7-tetraamino-1,8-dihydroxyanthracene-  
177 9,10-dione (4NADA) monomers in the polyimide chains can enhance the  
178 rigidity of the structure<sup>31</sup>.

179 A new dianhydride, 10-oxo-9-phenyl-9-(trifluoromethyl)-9,10-  
180 dihydroanthracene-2,3,6,7-tetraacid dianhydride (3FPODA), was proven to  
181 be an ideal candidate monomer for enhancing the adhesive properties and  
182 glass transition temperatures (T<sub>g</sub>) of colorless PI (Fig. 2I)<sup>32</sup>. One special  
183 flexible PI film obtained using a multicomponent copolymerization  
184 methodology from a fluoro-containing dianhydride, 4,4'-  
185 hexafluoroisopropylidene)diphthalic anhydride (6FDA), a rigid  
186 dianhydride, 3,3',4,4'-biphenyltetracarboxylic dianhydride (BPDA), and a  
187 fluoro-containing diamine, 2,2'-bis(trifluoromethyl)-4,4'-bis[4-(4-amino-  
188 3-methyl)benzamide]biphenyl (MABTFMB), showed good optical  
189 properties and excellent thermal properties (Fig. 2J)<sup>33</sup>.

190 It was concluded that the methods of PI synthesis are completely  
191 complicated. By changing the elements, the ratio of monomers, and the  
192 preparation method, hundreds of thousands of PIs with different  
193 characteristics can be obtained.

194 The application and popularization of PI could improve due to  
195 improvements in synthesis strategies and spinning technology.



### 3. Properties of PI as a biological/medical material

To be a biomedical polymer material, some basic characteristics need to be met. These include but are not limited to (1) being chemically inert, not due to contact with body fluids; (2) not causing inflammation or foreign body reactions to human tissues; (3) not causing cancer; (4) not clotting on the surface of the material, with antithrombotics; (5) long-term implantation in the body, with which the mechanical strength does not decrease; (6) being able to withstand the necessary cleaning and disinfection measures without degeneration; and (7) being easy to process into the required complex shape. It is worth mentioning that PI not only meets all the conditions of interest but also shows beneficial biological activity<sup>34, 35</sup>. The following characteristics are a list of the advantages of the PI used in the medical field.

#### 3.1 Long-term stability

PI and PI matrix nanocomposites have attracted increasing attention for material applications due to their high thermal stability at high temperatures. The thermogravimetric degradation profiles of pure PI show that the initial decomposition of PI occurs in the temperature range of 200-400°C because of the release of chemically bound water and evaporation of the solvent. The PI matrix achieved 40% mass loss at 500-630°C (Fig. 3A)<sup>36</sup>. The high-temperature resistance of the PI composite films was modified by integration with mica nanosheets (Fig. 3B)<sup>37</sup>. In a 20-month *in vitro* study, three commercially available PIs, U-Varnish-S (UBE, Japan), Durimim 7510 (FUJIFILM, Japan), and PI2611 (HD Microsystems, USA), were immersed in phosphate-buffered saline (PBS, pH=7.4) at special temperatures. After 20 months, the experimental PI did not undergo mass loss at 37°C (normal human body temperature) or 60°C (upper limit temperature for accelerated lifetime testing) in PBS, and the fracture mechanical properties, such as fracture energy, did not change (Fig. 3C-E)<sup>38</sup>. A new thin-film PI-based electrode array was stimulated by



226 electricity and then immersed in PBS at body temperature ( $37\pm 3^\circ\text{C}$ ) for 29  
227 d. The electrical characteristics were evaluated by cyclic voltammetry  
228 (CV), electrochemical impedance spectroscopy (EIS), and voltage  
229 transients (VT). The results showed the stable electrode material of the PI  
230 electrode array<sup>39</sup>. PBS obviously does not fully represent the complex  
231 environment in the body. Studies on the long-term biological stability of  
232 PI *in vivo* have also been reported. After being implanted in animals, the  
233 PI electrode can work stably for months or even a year<sup>40-42</sup>. Cross-  
234 sectional imaging using focused ion beam scanning electron microscopy  
235 (FIB-SEM) revealed well-adhered layers of the metallic electrode and PI,  
236 and no aging phenomena, such as delamination or cracking, occurred (Fig.  
237 3 F-H)<sup>40</sup>. Similar results were obtained after implantation of the PI  
238 material into rabbit eyes for 6 months. Light microscopy and SEM  
239 revealed that the PI materials did not obviously degrade (Fig. 3I)<sup>15</sup>. These  
240 results suggest that PI could be an ideal implanted material that maintains  
241 the dual stability of the PI itself and the implant environment.

### 242 3.2 Multiple Construction Process

243 PI is formulated in various forms, such as films, fibers, resins, foams,  
244 flexible electronic substrates, gas separation membranes, proton exchange  
245 membranes, and soluble PI, with different physical and chemical  
246 properties. Different forms of PI can be further modified to obtain  
247 thousands of properties according to different synthesis and processing  
248 processes, which gives PI great potential to be designed and manufactured  
249 with variable functionalities according to different requirements. For  
250 example, stiff forms of PI can be made into puncture needle-type devices  
251 (e.g., transverse intrafascicular multichannel electrodes)<sup>43</sup>, while neural  
252 electrodes attached to the cerebral cortex require flexible PI<sup>44</sup>. Different  
253 curing temperatures<sup>45</sup> and surface modifications<sup>46</sup> can change the  
254 hydrophobicity and roughness of PI materials. A smooth surface is  
255 suitable for the cardiovascular system and helps to reduce the risk of



256 thrombosis<sup>47</sup>, while a rough surface facilitates fibroblast and osteoblast  
257 attachment<sup>48</sup>. Changes in surface morphology can also strengthen the  
258 differentiation of mesenchymal stem cells into adipogenic and osteogenic  
259 lineages *in vitro*<sup>49</sup>, which can be applied in the field of wound repair. In  
260 addition, porous PI can be used as a drug delivery system. Different drugs  
261 can be loaded, and the release rate becomes controllable due to the  
262 different pore sizes of PI<sup>50</sup>. Excitingly, the features of multiple  
263 construction processes of PI provide an effective method to perform  
264 numerous chemical modifications that could be advanced to overcome the  
265 shortcomings of present materials.

### 266 3.3 Biocompatibility

267 Materials scientists recognize that "biocompatibility" is a characteristic of  
268 the material-biological host response system, not the property of the  
269 material itself in a specific application<sup>51</sup>. Cytotoxicity testing is an  
270 essential aspect of evaluating biocompatibility. Richardson et al. showed  
271 for the first time that PI has no cytotoxic effects on mouse fibroblast  
272 (Swiss-3T3) cells, similar to polytetrafluoroethylene (PTFE) and  
273 polydimethylsiloxane (PDMSO) (usually used as hydrophobic substrates  
274 for plaster drugs)<sup>52</sup>. After that, the cytotoxicity of PI to L929 mouse  
275 fibroblasts<sup>53</sup>, human retinal pigment cells (Fig. 4A)<sup>15</sup>, human epithelial  
276 cells (adherent HeLa)<sup>54</sup>, human cerebromicrovascular endothelial cells  
277 (hCMECs) (Fig. 4B)<sup>55</sup> and human dermal fibroblasts<sup>56</sup> was tested. Some of  
278 these studies claim to follow ISO standards strictly. Other studies have  
279 used 3-(4,5)-Dimethylthiazol-2-yl-2,5-diphenyltetrazolium bromide  
280 (MTT) assays, lactic dehydrogenase-based toxicology assays, calcein-AM,  
281 and ethidium bromide-based live/dead assays. All *in vitro* experiments  
282 suggested that PI has low/noncytotoxic effects.

283 Although investigators widely use cytotoxicity testing and are the only  
284 biocompatibility experiments for many biomaterial-related studies, it is  
285 obvious that *in vitro* studies of single cell lines and simple environments



286 are far from able to explain biocompatibility problems *in vivo*. As the  
287 understanding of biocompatibility has deepened, an increasing number of  
288 studies have begun to explore the hemocompatibility (i.e., does not cause  
289 hemolysis or coagulation) of PIs (Fig. 4C, 4D)<sup>57</sup>, genotoxicity<sup>58</sup>,  
290 irritation<sup>59</sup>, and host response<sup>60</sup>. New thin-film PI electrodes were also  
291 tested in biocompatibility studies, including acute systemic toxicity,  
292 irritation, pyrogenicity, sensitization, immune system response, and a  
293 prolonged 28-d subdural implant *in vivo* (Fig. 4E)<sup>61</sup>. In these studies,  
294 neither the PI nor implants with the PI as the main material were found to  
295 cause severe negative effects *in vitro* or *in vivo*. Fortunately, new thin-  
296 film PI electrodes were permitted by the US FDA for clinical trials  
297 [510(k) K192764], making it possible to use these electrodes as the first  
298 subdural electrode to develop rapidly from studies to the clinic, indicating  
299 that more long-term *in vivo* studies of PI are needed to prove its  
300 biocompatibility. However, a five-year safety study of minimally invasive  
301 glaucoma surgery showed that patients implanted with PI materials  
302 (Micro-Stent) experienced more endothelial cell loss over time than  
303 patients who underwent only standard cataract surgery (loss 20.4% vs.  
304 10.1%) (Fig. 4F)<sup>62</sup>. This suggests that more long-term *in vivo* studies of PI  
305 need to be performed due to the special PI materials with low cytotoxicity.

#### 306 **4. Medical applications of polyimides**

307 As one of the high-performance classes of polymers, an increasing number  
308 of studies have focused on broadening the applications of PI.

309 The superior high- or low-temperature tolerance, chemical solvent and  
310 radiation resistance, flexibility, dielectric properties, biocompatibility,  
311 long-term stability and multiple construction process properties of PI have  
312 made its use possible from industry to medicine. The medical applications  
313 of PIs are listed and summarized in Table 1.

#### 314 **4.1 PI electrodes in the nervous system**

315 Electrodes that function as signal collectors and transmitters are mainly



316 used in the study, diagnosis, and treatment of diseases. They have  
317 attracted much attention as important components of neuron-computer  
318 interfaces in recent years. For example, intracranial nerve electrodes  
319 collect raw physiological signals and are the most important part of the  
320 entire signal-processing process<sup>63</sup>. The integrated electrode itself needs to  
321 be long-lasting and stable while minimizing adverse effects on the  
322 organism to collect the clearest and most stable signal (Fig. 5A)<sup>40</sup>. The  
323 choice of substrate material is crucial. In this regard, the combination of  
324 the two properties of "flexibility" and "small cross-sectional area" seems  
325 to be particularly effective<sup>42, 64</sup>. PI, as an excellent material for meeting  
326 this requirement, has high potential to serve as an electrode in neural  
327 applications due to its biocompatibility<sup>64</sup>, electrochemical inertity<sup>42</sup>,  
328 electrical conductivity, and long-term stability (Fig. 5B)<sup>40</sup>. An increasing  
329 number of studies have investigated PIs with different backbones used for  
330 integrated microelectrodes (Fig. 5C)<sup>42</sup>.  
331 Microelectrodes fabricated from fully aromatic PIs show superior  
332 performance for the electrochemical monitoring of dopamine and provide  
333 evidence for the early diagnosis of neurological disorders<sup>65</sup>. A flexible PI is  
334 also used as a substrate to develop epidural electrocorticography  
335 electrodes, which can monitor various neurodegenerative diseases<sup>66</sup>. One  
336 PI-based flexible electrode can record electrocorticography signals in  
337 multiple regions with minimal invasiveness of the brain (Fig. 5D)<sup>67</sup>.  
338 Moreover, a brain intracranial electroencephalogram microdisplay  
339 engineered by the PI as a substrate to measure brain neuronal activity  
340 successfully identifies the boundaries of normal versus pathological brain  
341 regions and displays changes in near real-time on the surface of the brain  
342 in the surgical field<sup>68</sup>. The nanofabricated PI-based microelectrode for  
343 high-resolution mouse electroencephalography is a competent tool for  
344 recording large-scale brain activity and accommodating the ability to  
345 distinguish the neural correlates of certain brain waves in conjunction



346 with special behavior<sup>69</sup>. One special electrode that combines PI with  
347 prototype carbon records the signaling of the neural local field with an  
348 equal or better signal-to-noise ratio and almost completely removes image  
349 artifacts at magnetic fields of strength up to 9.4 T and is potentially useful  
350 for electrophysiology and magnetic resonance imaging for neurological  
351 diseases<sup>70</sup>. In addition, PI electrodes are also applied for recording output  
352 signals in human nerves in the robotic arms of amputees<sup>71</sup>. The  
353 photosensitive PI microelectrode arrays (epiretinal bio-MEAs) lying on  
354 the visual cortex in the eyes of rabbits successfully recorded the response  
355 to electrical stimuli (Fig. 5E)<sup>15</sup>.

356 Furthermore, electrical neuron stimulation also provides promising  
357 methods for treating and diagnosing chronic neurological diseases, such as  
358 epilepsy. New thin-film PI electrodes for use in clinical trials for surgical  
359 evaluation of patients with drug-resistant epilepsy have been announced  
360 only by the FDA<sup>61</sup>. A microlight-emitting diode array with a flexible PI  
361 film used as a chronic photostimulation unit and a whole-cortex  
362 electrocorticographic electrode used as a recording unit were implanted  
363 into the cerebral cortex of common marmosets for 4 months. This device  
364 gradually increased neural responses after photostimulation for ~8 weeks  
365 <sup>72</sup> and has potential applications for epilepsy treatment. In peripheral  
366 nerves, PI-based implantable flexible microelectrode arrays (MEAs),  
367 which provide nerve stimulation and recording on the surface of long-term  
368 denervated muscles, can reduce the atrophy of denervated muscle while  
369 retaining more acetylcholine receptors<sup>73</sup>. One transverse intrafascicular  
370 multichannel electrode was transversally implanted into the rat sciatic  
371 nerve and the median human nerve to interface with the peripheral nerve  
372 (Fig. 5F-G)<sup>43</sup>. The PI-based MEAs can be further used for the stimulation  
373 of remaining retinal neurons in patients with degenerated photoreceptors  
374 <sup>15, 74</sup>.

375 However, mice implanted with PI-based microelectrodes on free muscle





376 flap grafts and subjected to electrical stimulation for 6 weeks exhibited an  
377 increased inflammatory response, myopathy, and partial necrosis<sup>75</sup>. These  
378 studies suggested that the multiple functionalities of PI electrodes provide  
379 exciting opportunities for fundamental neuroscience studies, as well as for  
380 stimulation-based neural therapies, but future work should carefully  
381 investigate the optimal electrode material, graft, and stimulated phase.

#### 382 **4.2 PI in biosensors**

383 Implantable or noninvasive biosensors used as real-time monitors are  
384 powerful devices for diagnosing and predicting disease and maintaining  
385 human health by monitoring and providing continuous or regular biometric  
386 signals. Like neural electrodes, biosensors (which transmit physical or  
387 chemical signals) often use PI as a sensor substrate because of its good  
388 biocompatibility, hemocompatibility, and other properties. PIs were  
389 fabricated as thin, flexible, and implantable neuroprobes with aptamer-  
390 field-effect transistor biosensors for neurochemical signaling monitoring  
391<sup>18</sup>. PI has been applied in interventional procedures, such as real-time  
392 monitoring of cerebral aneurysm hemodynamics (Fig. 6A)<sup>76</sup>. The  
393 microphone array integrated into the PI can be used to qualify  
394 hemodialysis vascular access dysfunction (location and degree of stenosis)  
395 (Fig. 6B)<sup>77</sup>. A novel biosensor that manufactured an array of 64 hybrid  
396 cantilevers with a PI substrate detected drug-induced adverse effects at  
397 early stages, such as depolarization and Torsade de Points, in  
398 cardiomyocytes (Fig. 6C)<sup>16</sup>. One miniature fiber optic pressure sensor  
399 fabricated with PI, which is tiny enough to be implanted into rodent discs  
400 without changing the structure or changing the intradiscal pressure, was  
401 first successfully applied for rodent intradiscal pressure measurements  
402 (Fig. 6D)<sup>78</sup>. Furthermore, a multichannel temperature sensor fabricated from  
403 a flexible PI film can wrap around a dental implant abutment wing and  
404 then send real-time warning signals before failure of the implant (Fig.  
405 6E)<sup>79</sup>.



406 It has also been reported that biosensors made with PI as a substrate have  
407 excellent abilities for trace-level or specific detection of the  
408 concentrations of some hormones, glucose, and gases produced by the  
409 body or others. One flexible biosensor was prepared by direct synthesis of  
410 molybdenum disulphide (MoS<sub>2</sub>) on a PI substrate, which can be  
411 sensitively used for the determination of endocrinopathy by measuring  
412 endocrine-related hormones, such as parathyroid hormone (PTH),  
413 triiodothyronine (T3), and thyroxine (T4), in clinical patient sera<sup>80</sup>.  
414 Ultrasensitive sensor arrays on PI substrates can be used for multiplexed  
415 and simultaneous electrochemical detection of cardiac damage markers,  
416 cardiac troponin-I (cTnI) and cardiac troponin-T (cTnT), in human  
417 serum<sup>81</sup>. A porous PI film sensor combined with grafted MgO-templated  
418 carbon can be applied to sensitively measure acetaldehyde gas released by  
419 human skin, even at low concentrations<sup>82</sup>. A special human sweat-based  
420 wearable glucose sensor microfabricated with reduced graphene oxide on a  
421 flexible PI substrate and integrated chitosan-glucose oxidase composites  
422 exhibited sensitive, rapid, and stable response performance for detecting  
423 glucose from human sweat (Fig. 6F)<sup>83</sup>.  
424 A PI-based film bulk acoustic resonator (PI-FBAR) humidity sensor  
425 operating for the first time was utilized for detecting human respiratory  
426 rates in real-time *in vitro* (Fig. 6G)<sup>84</sup>. One biosensor made of highly porous  
427 graphitic carbon electrodes fabricated with commercial PI tape offers  
428 rapid, low-cost, time-saving, selective, and sensitive electrochemical  
429 detection for point-of-care analysis of cytokines such as IL6<sup>85</sup>. In  
430 addition, neuronal cells were generated on biosensors printed with few-  
431 layer graphene ink onto Kapton PI to evaluate the electrophysiology and  
432 electrical signaling of Parkinson's disease *in vitro*<sup>86</sup>. Lin R. et al. reported  
433 that an ultrathin PI microsensor array can be integrated into a puncture  
434 needle for early detection of small volumes of blood extravasation (Fig.  
435 6H)<sup>87</sup>. As a small spring constant of PI, PI/Si/SiO<sub>2</sub>-based piezoresistive



436 microcantilever biosensors were developed to sensitively and precisely  
437 detect aflatoxin B1 in various foods and other biomolecules<sup>88</sup>. Sensors  
438 integrated with PI as substrates have the potential to satisfy the need for  
439 innovative examination or analytic platforms owing to their high  
440 throughput, sensitivity, biocompatibility, and simplified data analysis.

#### 441 **4.3 PI in drug delivery systems**

442 Drug modifications, microenvironmental modifications, and drug delivery  
443 systems are the three core paradigms of drug delivery technology. Drug  
444 delivery systems can build an interface between the drug and its  
445 microenvironment, adjusting and optimizing the activity of the drug<sup>17</sup>.  
446 Polymers generated by the PI form the basis of many drug delivery  
447 systems for multiple functions, such as controlled release and targeted  
448 release. Lumen drug-loaded PI tubing with micro-holes in the tube wall  
449 has been made into a diffusion-controlled reservoir-type implantable  
450 device<sup>89</sup>. The device was implanted subcutaneously in mice and achieved  
451 stable drug release for several months (Fig. 7A)<sup>90</sup>. Microneedles are an  
452 advanced transdermal drug delivery system. The introduction of PI can  
453 increase the mechanical strength of microneedle arrays of carbon  
454 nanotubes, providing skin penetration with a smaller insertion force (Fig.  
455 7B)<sup>91, 92</sup>. In interventional surgery, PI microcatheter-oriented cephalad in  
456 the internal carotid artery allows for reproducible delivery of drugs to the  
457 ipsilateral cerebral hemisphere (Fig. 7C)<sup>93</sup>. The drugs gentamicin,  
458 dexamethasone, and lidocaine can be delivered to the tympanic chamber  
459 through PI microtubing at the round window membrane into the cochlea<sup>94</sup>.  
460 One special covalent organic framework (COF) synthesized from PI  
461 loaded with ibuprofen exhibited high drug loading and well-controlled  
462 release (Fig. 7D)<sup>50</sup>. PI-based transdermal skin patches have been applied  
463 for the controlled release of ondansetron after chemotherapy<sup>95</sup>. Similarly,  
464 PI and reduced graphene oxide composite transdermal patches have also  
465 been used in insulin delivery (Fig. 7E)<sup>96</sup>. Additionally, flexible PI probes



466 can be used for highly localized drug delivery and can be applied to study  
467 electrical and chemical information exchange and communication between  
468 cells both *in vitro* and *in vivo* (Fig. 7F)<sup>97</sup>.

469 The PI-based drug delivery device is a promising way to establish precise,  
470 high-volume loading, good release control, and safety for drug delivery  
471 applications.

#### 472 **4.4 PI in bone tissue replacements and artificial muscles**

473 It is universally acknowledged that metallic materials are the most  
474 commonly used implants for load-bearing bone repair<sup>98</sup>. However, metallic  
475 implants with a high elastic modulus have stress-shielding effects that  
476 result in bone resorption and bone atrophy, leading to loosening or failure  
477 of the implants<sup>99</sup>. Due to their relative inertness, superior mechanical  
478 strength, elastic modulus, bioactivity, and biocompatibility, PI  
479 biomaterials are attractive materials that could be applied to bone tissue  
480 and joint replacement candidates for replacing traditional cartilage  
481 materials. The biological inertness of PI indicates a reduced inflammatory  
482 response. However, PI, a bioinert material used as a bone substitute,  
483 cannot induce a cell response, bone development and repair or  
484 osteointegration, which are important foundations for eventual bone  
485 healing<sup>100</sup>.

486 To resolve this problem, the surface bioactive properties of PI for  
487 potential bone substitutes have improved [38]. Kaewmanee et al. used  
488 concentrated sulfuric acid to treat PI, creating microporous surface  
489 phenotypes on the materials. At the same time, flower-like molybdenum  
490 disulphide submicron-spheres added to sulfuric acid in advance are  
491 attached to the microporous surface of PI, resulting in the final PI-  
492 molybdenum disulphide composites, which exhibit good osteogenic and  
493 antibacterial functions (Fig. 8A-F)<sup>101</sup>. Moreover, the microporous PI  
494 coating with 15 w% tantalum oxide submicron-particles resulted in greater  
495 bioactivity, and cellular responses (such as proliferation, adhesion, and



496 alkaline phosphatase activity) were induced by bone marrow stromal cells  
497 from rats (Fig. 8G-L)<sup>102</sup>. In particular, Zhang et al. reported that 40 W%  
498 nanolaponite ceramic fabricated with PI through melt processing could  
499 increase the bioactivity of PI as an implantable material for bone repair.  
500 The greater amount of apatite deposited on this composite material  
501 indicates good bioactivity; it exhibited outstanding proliferation, cell  
502 adhesion, and alkaline phosphatase activity in rat bone mesenchymal stem  
503 cells *in vitro* and remarkably induced osteogenesis and osseointegration in  
504 male beagle dogs *in vivo* (Fig. 8M-O)<sup>103</sup>.

505 In addition to bone substitutes, PI is also used in the design of artificial  
506 muscles. Ling et al. added a corrugated grid-like PI scaffold inside a  
507 muscle prosthesis to simulate the undulated perimysial collagen fibers  
508 surrounding the myocardium, making the contraction of the muscle  
509 prosthesis direction-dependent and more in line with physiological  
510 conditions<sup>104</sup>.

511 Overall, these findings show that this bioengineering approach involving  
512 PI provides promising strategies for fabricating biomimetic bone  
513 substitutes for bone repair and muscle reconstruction.

#### 514 **4.5 PI in face masks or respirators**

515 The traditional N95 mask provides 85% protection for sub300 nm  
516 particles. Unfortunately, it cannot meet the demand to protect against  
517 pathogens such as the COVID-19 virus, which has a diameter of 65-125  
518 nm<sup>105</sup>. Since the outbreak of COVID-19 across the globe, antipathogen  
519 mask design and decontamination methods involving N95/N99 masks have  
520 been preferentially studied and developed<sup>106</sup>. By utilizing the  
521 hydrophobicity and low pore size (down to 5 nm) of PI nanofiber  
522 membranes, investigators have focused on the outstanding filter performance  
523 of PI materials. PI electrospun fibers with embedded metal-organic  
524 frameworks are made to mask and perform well at filtering volatile  
525 organic compounds represented by formaldehyde<sup>107</sup>. Polyimide and



526 polyethersulfone solutions have been used in electrospinning to develop  
527 nanofiber membranes with excellent filtration efficiency for particulate  
528 matter, excellent filter quality for nano-aerosols, excellent interception  
529 ratios for bacteria and viruses (above 99%), and nontoxic effects on cells  
530 <sup>108</sup>. In addition, PI has also been introduced into the design of  
531 photothermal self-purification masks. With the help of plasmonics, the  
532 surface temperature of the respirators increases to more than 80°C within  
533 1 min after exposure to sunlight, enabling convenient inactivation and  
534 reuse of microorganisms <sup>109</sup>. However, in the study of Ghatak et al., PI-  
535 nylon did not show a superior triboelectric ability to latex rubber<sup>110</sup>.  
536 Crucially, the low price of raw materials makes the mass generation of PI-  
537 based masks feasible. This finding suggested that the filtration efficiency  
538 of the PI mask against bacteria, viruses, volatile organic compounds, and  
539 polluted air needs to be confirmed before use.

#### 540 **4.6 PI as an antibacterial material**

541 The reported experimental results showed that the antibacterial ability  
542 includes antibacterial adhesion, antibacterial biofilm formation, inhibition  
543 of bacterial growth under coculture, and accelerated wound healing of  
544 infection.

545 It is worth noting that some studies exploring the antimicrobial effect of  
546 PI composites have only tested the antimicrobial ability of the composite  
547 as a whole and have not tested PI alone, where PI is considered a  
548 hydrophobic matrix/carrier and the antimicrobial activity defaults to its  
549 non-PI component<sup>101</sup>. It has also been found that the PI used in composite  
550 materials exhibits low antibacterial activity<sup>102, 111, 112</sup>. PIs modified with a  
551 concentrated sulfuric acid suspension containing 15% tantalum oxide  
552 submicron-particles (named PIST15) exhibited improved antibacterial  
553 properties<sup>102</sup>. Topographically and chemically modified commercial PI  
554 films (Kapton, American) improved the antibacterial properties of these  
555 materials, decreasing bacterial *Pseudomonas aeruginosa* (*P. aeruginosa*)



556 adhesion and inhibiting bacterial growth but not triggering cell death in  
557 the attached bacteria<sup>113</sup>.

558 Recently, there have been successful studies in which only PI was used to  
559 make antibacterial medical catheters and dressings (here, PI is not a  
560 matrix of composite antimicrobial materials). Lee et al. developed a  
561 surface-modified medical PI catheter that forms an antifouling layer, as its  
562 surface is modified with hydrophilic amino acids. *In vitro* experiments  
563 have shown that the adhesion of bacteria, fibrinogen, and albumin on the  
564 surface of the duct decreases significantly, which is highly important for  
565 the prevention of catheter-associated infections<sup>114</sup>. Polymer films based on  
566 2-methacryloyloxyethyl phosphorylcholine-modified hyperbranched PI  
567 synthesized directly significantly reduced the number of adhesive bacteria  
568 and improved the antibacterial properties in *in vitro* experiments<sup>115</sup>. The  
569 CuFe<sub>2</sub>O<sub>4</sub>@SiO<sub>2</sub>-PI nanoparticles exhibited good biocompatibility with  
570 HEK293T cells and antibacterial properties against *P. aeruginosa*,  
571 *Escherichia coli* (*E. coli*), and *Staphylococcus aureus* (*S. aureus*)<sup>116</sup>. In  
572 our group, wound dressings made of PI fibers showed significant  
573 antimicrobial effects on methicillin-resistant *S. aureus* (MRSA) and *E.*  
574 *coli* in *in vitro* experiments. It was found that the PI fibers directly  
575 damaged the cell walls of both bacteria. *In vivo*, PI dressings effectively  
576 improved local infection of smeared wounds in mice, inhibited the  
577 bacterial load, reduced infiltrating macrophages, and accelerated the  
578 healing of pathogen-infected wounds<sup>34</sup>. We used other forms of PI  
579 materials with similar original materials, but different polymerization  
580 reactions were used to investigate the antibacterial properties of these  
581 materials (Fig. 9). However, specific PI fibers exhibit significant  
582 antibacterial effects *in vitro*<sup>34</sup>.

583 Studies have shown that PI materials have excellent antibacterial  
584 properties and possess many other advantages, such as biocompatibility,  
585 long life, and reusability. These successful examples may indicate that PI



586 antimicrobial materials are expected to be applied in the clinic in the near  
587 future.

## 588 **5. Trends and Outlook**

589 Recent progress in controlled polymerization has led to the development  
590 of diverse, complex composites for various applications. PI is considered  
591 to be one of the polymer materials with the best overall performance and  
592 has been broadly investigated due to its unique features and application in  
593 advanced materials. However, apart from the great amount of progress  
594 summarized in the present review, some challenges still need to be met for  
595 PI technology in either theoretical or practical aspects in medical areas in  
596 the future for translating PI materials into practical applications.

597 Methods to control the appearance, characteristics, and function of PIs for  
598 medical applications have been developed. Synthesizing composite  
599 materials and changing the inherent properties of PIs are possible ways to  
600 improve the application range of PIs. With current technology, it is easy  
601 to change some properties of PI, such as morphology, hardness, thermal  
602 conductivity, and insulation. However, with the rapid development of the  
603 medical field of polymers, both *in vitro* and *in vivo*, more PIs with better  
604 performance will be developed. For example, improving the electrical  
605 feasibility of insulation PIs has attracted increasing attention. Conductive  
606 materials offer advantages, such as complex conductive biomaterial-based  
607 wound dressings with conductivity similar to that of human skin, which  
608 can significantly enhance wound healing.

609 As the complexity of electrodes increases, the challenges associated with  
610 their manufacture and clinical applications also increase. Overcoming the  
611 damage to tissue by electrode implantation, inevitable glial scarring,  
612 inflammation, and neuronal loss accompanying all implantable  
613 neurotechnologies within months remains the greatest demand.

614 Furthermore, to protect the functional neuronal circuitry near electrodes, a  
615 great deal of effort has been invested in improving the biocompatibility of





616 neural probes.

617 As sensors, these challenges include detecting analyte concentrations at  
618 ultralow levels (down to parts per billion or nanomolar levels), coping  
619 with complex sample matrices containing numerous interfering species,  
620 addressing issues related to differentiating isomers and structural analogs  
621 and managing intricate, multidimensional data sets. Advanced artificial  
622 intelligence techniques, including machine learning, could help boost the  
623 performance of these kinds of sensors for medical applications,  
624 nanotoxicology, neural prostheses, wireless technology, smart agriculture,  
625 environmental monitoring, and advanced medical manufacturing  
626 technologies.

627 There is an urgent need for modified industrial and medical masks that  
628 provide additional air filtration and deactivate pathogens using various  
629 technologies. Polymers with inherent micropores in the fiber matrix  
630 perform better in filtration, among which filter membranes based on PI  
631 fibers featuring macro, meso-, and micropores and good filtration  
632 efficiency have been designed. Investigators are also trying to use the  
633 electrical energy generated by the self-friction of masks to directly kill  
634 pathogens or provide electricity for sensors and antipathogen devices.

635 Researchers have investigated the cytotoxicity of PI, particularly the fate  
636 of PI when it interacts with mammalian cells or is implanted *in vivo*.

637 Comprehending this area will lead to the development of next-generation  
638 PI medical materials that confirm safety guarantees for clinical  
639 applications.

## 640 **6. Conclusion**

641 The demands for biomaterials and medical devices have attracted attention  
642 recently worldwide. The safety and performance of these materials should  
643 be a priority when considering the conditions and the environment that  
644 would most benefit patients in repairing organ functions. PI is one of the  
645 most important high-performance and advanced polymers. In this review,



646 we introduce the chemical composition, structural features, spinning  
 647 solutions, and reaction mechanism and then summarize the properties of  
 648 PI and its practical applications. It was suggested that different forms of  
 649 PI, including power, films, fibers, resins, foams, and soluble PI, have  
 650 different characteristics and applications. PIs have been studied and  
 651 manufactured as neural electrodes, sensors, drug delivery systems, tissue  
 652 replacements, masks, antimicrobial catheters, and antimicrobial dressings  
 653 in healthcare. Overall, this review will form a design guideline for future  
 654 PI materials/devices and help investigators overcome the obstacles to  
 655 further functional improvement for PI applications in the medical field.

### 656 **Conflicts of interest**

657 There are no conflicts of interest to declare.

### 658 **Acknowledgments**

659 This research was supported by the Specialized Program (NO. 2022-JCJQ-  
 660 ZD-224-12) and the Chongqing Talent Project (NO. Cstc2021ycjh-  
 661 bgzxm0340). We want to thank Prof. Zheng Chunfu for helpful  
 662 discussions and for polishing the grammatical presentation of this  
 663 manuscript.

664 Table 1. Summary of the medical applications of PI.

<b>Applications</b>	<b>Devices</b>	<b>Functions</b>
<b>Neural Electrodes</b>	Electrocorticography (ECoG) arrays	Dopamine monitoring <sup>65</sup> , high-Performance neural recordings <sup>61, 66, 67, 69</sup> , pathological brain regions identification <sup>68</sup> , chronic stimulation <sup>72</sup>
	Peripheral electrodes	Epiretinal stimulation <sup>15</sup> , motor nerve stimulation <sup>43</sup> , denervated muscles stimulation <sup>73</sup> , afferent nerve stimulation <sup>71</sup>
	Depth probes	Brain-computer interface <sup>40</sup> , chronic stimulation and monitoring <sup>42</sup>
<b>Biosensor</b>	Vessel-related sensors	Aneurysm monitoring <sup>76</sup> , stenosis monitoring <sup>77</sup> , extravasation detection <sup>87</sup>



	<i>In vitro</i> sensors	Cells' electrical signaling sensing <sup>86</sup> , electrochemical detection <sup>85</sup>	<a href="#">View Article Online DOI: 10.1039/D4NA00292J</a>
	Implant sensors	Intradiscal pressure measurement <sup>78</sup> , dental implant detection <sup>79</sup>	
<b>Drug Delivery Systems</b>	PI tubes	Controlled-release subcutaneously <sup>89</sup> , inner ear drug delivery <sup>94</sup> , intracranial drug delivery <sup>93</sup>	
	Microneedles	Painless subcutaneous drug delivery <sup>91,92</sup>	
	transdermal patches	Electrothermal and photothermal triggered drug release <sup>95,96</sup>	
	PI-COF	High drug loading and well-controlled release <sup>50</sup>	
<b>Tissue Replacements</b>	Artificial bones	Osteogenesis and osseointegration inducing <sup>101,103,111</sup>	
	Artificial muscle	Simulating perimysial collagen fibers <sup>104</sup>	
<b>Respirators</b>	Medical masks	Self-friction generating electric energy <sup>117</sup> , photothermal self-purification <sup>109</sup>	
<b>Antibacterial Material</b>	Medical catheter	Anti-biofilm formation <sup>114</sup> ,	
	Anticoagulant membrane	Antibacterial adhesion <sup>115</sup>	
	Dressing	Bacteria killing and healing promoting <sup>34</sup>	

665

666

667

668

669

670

671

672

673

674

675

676

677

678



679

680

681

682

683

684 **References**

- 685 1. L. De Laporte and F. Kiessling, *Advanced Healthcare Materials*, 2023, **12**,
- 686 2301637.
- 687 2. M. Wilczynski, O. Wilczynska and W. Omulecki, *Klin Oczna*, 2009, **111**, 21–25.
- 688 3. Y. Wang, Y. Liu, Q. Han, H. Lin and F. Liu, *J Memb Sci*, 2022, **649**, 120359.
- 689 4. D. Y. Fuhrman, E. K. Stenson, I. Alhamoud, R. Alobaidi, G. Bottari, S.
- 690 Fernandez, F. Guzzi, T. Haga, A. Kaddourah, E. Marinari, T. H. Mohamed, C.
- 691 J. Morgan, T. Mottes, T. M. Neumayr, N. J. Ollberding, V. Raggi, Z. Ricci,
- 692 E. See, N. L. Stanski, H. Zang, E. Zangla, K. M. Gist and W. -R.
- 693 Investigators, *JAMA Netw Open*, 2024, **7**, e240243.
- 694 5. E. H. Leung, A. Gibbons and D. D. Koch, *Ophthalmology*, 2020, **127**, 859–865.
- 695 6. A. Garcia and N. D. Giraldo, *Biomedica*, 2022, **42**, 707–716.
- 696 7. A. Shariati, S. M. Hosseini, Z. Chegini, A. Seifalian and M. R. Arabestani,
- 697 *Biomed Pharmacother*, 2023, **158**, 114184.
- 698 8. Y. Tamura and T. Abe, *Clin Case Rep*, 2023, **11**, e7276.
- 699 9. E. Spaziani, A. Di Filippo, P. Francioni, M. Spaziani, A. De Cesare and M.
- 700 Picchio, *Acta Chir Belg*, 2018, **118**, 48–51.
- 701 10. L. Wang, M. Xin, M. Li, T. Zhang, Y. Pang and Y. Mao, *Carbohydr Res*, 2024,
- 702 **538**, 109078.
- 703 11. S. Ma, S. Wang, S. Jin, Y. Wang, J. Yao, X. Zhao and C. Chen, *Polymer*,
- 704 2020, **210**.
- 705 12. Y. Zhang, Z. Huang, B. Ruan, X. Zhang, T. Jiang, N. Ma and F. C. Tsai,
- 706 *Macromol Rapid Commun*, 2020, **41**, e2000402.
- 707 13. K. Choi, A. Droudian, R. M. Wyss, K. P. Schlichting and H. G. Park, *Sci*
- 708 *Adv*, 2018, **4**, eaau0476.
- 709 14. H. S. Bi, X. X. Zhi, P. H. Wu, Y. Zhang, L. Wu, Y. Y. Tan, Y. J. Jia, J. G.
- 710 Liu and X. M. Zhang, *Polymers (Basel)*, 2020, **12**.
- 711 15. X. Jiang, X. Sui, Y. Lu, Y. Yan, C. Zhou, L. Li, Q. Ren and X. Chai, *J*
- 712 *Neuroeng Rehabil*, 2013, **10**, 48.
- 713 16. D. S. Kim, Y. J. Jeong, A. Shanmugasundaram, N. E. Oyunbaatar, J. Park, E.
- 714 S. Kim, B. K. Lee and D. W. Lee, *Biosens Bioelectron*, 2021, **190**, 113380.
- 715 17. A. M. Vargason, A. C. Anselmo and S. Mitragotri, *Nat Biomed Eng*, 2021, **5**,
- 716 951–967.
- 717 18. C. Zhao, T. Man, Y. Cao, P. S. Weiss, H. G. Monbouquette and A. M. Andrews,
- 718 *ACS Sens*, 2022, **7**, 3644–3653.



- 719 19. X. Dong, L. Chen, J. Liu, S. Haller, Y. Wang and Y. Xia, *Sci Adv*, 2016, **2**, e1501038. View Article Online  
DOI: 10.1039/D4NA00292J
- 720
- 721 20. M. Kanno, H. Kawakami, S. Nagaoka and S. Kubota, *J Biomed Mater Res*, 2002,
- 722 **60**, 53–60.
- 723 21. S. A. Tharakan and S. Muthusamy, *RSC Adv*, 2021, **11**, 16645–16660.
- 724 22. M. Zhang, H. Niu and D. Wu, *Macromol Rapid Commun*, 2018, **39**, e1800141.
- 725 23. T. Rensch, S. Fabig, S. Gratz and L. Borchardt, *ChemSusChem*, 2022, **15**,
- 726 e202101975.
- 727 24. A. E. Soldatova, R. N. Shamsutdinova, T. V. Plisko, K. S. Burts, A. Y.
- 728 Tsegelskaya, D. A. Khanin, K. Z. Monakhova, T. S. Kurkin, A. V.
- 729 Bildyukevich and A. A. Kuznetsov, *Materials (Basel)*, 2022, **15**.
- 730 25. W. Yang, F. Liu, H. Chen, X. Dai, W. Liu, X. Qiu and X. Ji, *Polymers*
- 731 *(Basel)*, 2020, **12**.
- 732 26. Z. Chang, X. Sun, Z. Liao, Q. Liu and J. Han, *Polymers (Basel)*, 2022, **14**.
- 733 27. G. Vaganov, M. Simonova, M. Romasheva, A. Didenko, E. Popova, E. Ivan'kova,
- 734 A. Kamalov, V. Elokhovskiy, V. Vaganov, A. Filippov and V. Yudin, *Polymers*
- 735 *(Basel)*, 2023, **15**.
- 736 28. X. Xiao, D. Kong, X. Qiu, W. Zhang, Y. Liu, S. Zhang, F. Zhang, Y. Hu and
- 737 J. Leng, *Sci Rep*, 2015, **5**, 14137.
- 738 29. L. Yu, Y. Yu, J. Shi, X. Zhang, F. Gao, C. Li, Z. Yang and J. Zhao,
- 739 *Polymers (Basel)*, 2022, **14**.
- 740 30. Y. Zi, D. Pei, J. Wang, S. Qi, G. Tian and D. Wu, *Polymers (Basel)*, 2021,
- 741 **13**.
- 742 31. B. Liu, Y. Zhou, L. Dong, Q. Lu and X. Xu, *iScience*, 2022, **25**, 105451.
- 743 32. Y. Wang, X. Liu, J. Shen, J. Zhao and G. Tu, *Polymers (Basel)*, 2022, **14**.
- 744 33. X. Ren, H. Wang, X. Du, H. Qi, Z. Pan, X. Wang, S. Dai, C. Yang and J. Liu,
- 745 *Materials (Basel)*, 2022, **15**.
- 746 34. X. Yang, W. Ma, H. Lin, S. Ao, H. Liu, H. Zhang, W. Tang, H. Xiao, F. Wang,
- 747 J. Zhu, D. Liu, S. Lin, Y. Zhang, Z. Zhou, C. Chen and H. Liang, *Nanoscale*
- 748 *Adv*, 2022, **4**, 3043–3053.
- 749 35. I. Antanaviciute, L. Simatonis, O. Ulcinas, A. Gadeikyte, B. Abakeviciene,
- 750 S. Tamulevicius, V. Mikalayeva, V. A. Skeberdis, E. Stankevicius and T.
- 751 Tamulevicius, *J Tissue Eng Regen Med*, 2018, **12**, e760–e773.
- 752 36. C. Akinyi and J. O. Iroh, *Polymers (Basel)*, 2023, **15**.
- 753 37. X. F. Pan, B. Wu, H. L. Gao, S. M. Chen, Y. Zhu, L. Zhou, H. Wu and S. H.
- 754 Yu, *Adv Mater*, 2022, **34**, e2105299.
- 755 38. B. Rubehn and T. Stieglitz, *Biomaterials*, 2010, **31**, 3449–3458.
- 756 39. S. Ong, A. Kullmann, S. Mertens, D. Rosa and C. A. Diaz-Botia,
- 757 *Micromachines (Basel)*, 2022, **13**.
- 758 40. C. Bohler, M. Vomero, M. Soula, M. Voroslakos, M. Porto Cruz, R. Liljemalm,
- 759 G. Buzsaki, T. Stieglitz and M. Asplund, *Adv Sci (Weinh)*, 2023, **10**,
- 760 e2207576.
- 761 41. A. Kiliyas, Y. T. Lee, U. P. Froriep, C. Sielaff, D. Moser, T. Holzhammer,
- 762 U. Egert, W. Fang, O. Paul and P. Ruther, *J Neural Eng*, 2021, **18**.



- 763 42. M. Vomero, F. Ciarpella, E. Zucchini, M. Kirsch, L. Fadiga, T. Stieglitz  
764 and M. Asplund, *Biomaterials*, 2022, **281**, 121372.
- 765 43. T. Boretius, J. Badia, A. Pascual-Font, M. Schuettler, X. Navarro, K.  
766 Yoshida and T. Stieglitz, *Biosens Bioelectron*, 2010, **26**, 62–69.
- 767 44. E. Otte, A. Vlachos and M. Asplund, *Cell Tissue Res*, 2022, **387**, 461–477.
- 768 45. Y. Sun, S. P. Lacour, R. A. Brooks, N. Rushton, J. Fawcett and R. E.  
769 Cameron, *J Biomed Mater Res A*, 2009, **90**, 648–655.
- 770 46. W. Ma, Y. Ding, M. Zhang, S. Gao, Y. Li, C. Huang and G. Fu, *J Hazard*  
771 *Mater*, 2020, **384**, 121476.
- 772 47. Y. Liang, M. Ernst, F. Brings, D. Kireev, V. Maybeck, A. Offenhausser and  
773 D. Mayer, *Adv Healthc Mater*, 2018, **7**, e1800304.
- 774 48. M. Voisin, M. Ball, C. O’Connell and R. Sherlock, *Nanomedicine*, 2010, **6**,  
775 35–43.
- 776 49. G. Abagnale, M. Steger, V. H. Nguyen, N. Hersch, A. Sechi, S. Joussem, B.  
777 Denecke, R. Merkel, B. Hoffmann, A. Dreser, U. Schnakenberg, A. Gillner and  
778 W. Wagner, *Biomaterials*, 2015, **61**, 316.
- 779 50. Q. Fang, J. Wang, S. Gu, R. B. Kaspar, Z. Zhuang, J. Zheng, H. Guo, S. Qiu  
780 and Y. Yan, *J Am Chem Soc*, 2015, **137**, 8352–8355.
- 781 51. M. Kowalczyk, *Polymers (Basel)*, 2020, **12**.
- 782 52. R. R. Richardson, Jr., J. A. Miller and W. M. Reichert, *Biomaterials*, 1993,  
783 **14**, 627–635.
- 784 53. D. Serbezeanu, T. Vlad-Bubulac, D. Rusu, G. G. Pircalabioru, I. Samoila, S.  
785 Dinescu and M. Aflori, *Materials (Basel)*, 2019, **12**.
- 786 54. S. Nagaoka, K. Ashiba and H. Kawakami, *Artif Organs*, 2002, **26**, 670–675.
- 787 55. P. Starr, C. M. Agrawal and S. Bailey, *J Biomed Mater Res A*, 2016, **104**,  
788 406–412.
- 789 56. A. M. Feldweg, D. S. Friend, J. S. Zhou, Y. Kanaoka, M. Daheshia, L. Li, K.  
790 F. Austen and H. R. Katz, *Eur J Immunol*, 2003, **33**, 2262–2268.
- 791 57. L. I. Buruiana, A. I. Barzic, I. Stoica and C. Hulubei, *Journal of Polymer*  
792 *Research*, 2016, **23**, 217.
- 793 58. E. Efsa Panel on Food Contact Materials, A. Processing, V. Silano, J. M.  
794 Barat Baviera, C. Bolognesi, A. Chesson, P. S. Cocconcelli, R. Crebelli, D.  
795 M. Gott, K. Grob, C. Lambre, E. Lampi, M. Mengelers, A. Mortensen, I. L.  
796 Steffensen, C. Tlustos, H. Van Loveren, L. Vernis, H. Zorn, L. Castle, E.  
797 Di Consiglio, R. Franz, N. Hellwig, M. R. Milana, K. Pfaff, K. Volk and G.  
798 Riviere, *EFSA J*, 2020, **18**, e06183.
- 799 59. C. Y. Lin, W. S. Lou, J. C. Chen, K. Y. Weng, M. C. Shih, Y. W. Hung, Z. Y.  
800 Chen and M. C. Wang, *Micromachines (Basel)*, 2020, **11**.
- 801 60. L. J. Shen, Y. Q. Chen, D. Cheng, C. Zhang, L. Jiang, M. Hong and Q. Y.  
802 Kang, *Curr Eye Res*, 2016, **41**, 79–87.
- 803 61. A. Kullmann, D. Kridner, S. Mertens, M. Christianson, D. Rosa and C. A.  
804 Diaz-Botia, *Front Neurosci*, 2022, **16**, 876877.
- 805 62. J. H. Lass, B. A. Benetz, J. He, C. Hamilton, M. Von Tress, J. Dickerson  
806 and S. Lane, *Am J Ophthalmol*, 2019, **208**, 211–218.



- 807 63. X. Strakosas, H. Biesmans, T. Abrahamsson, K. Hellman, M. S. Ejneby, M. J. Donahue, P. Ekstrom, F. Ek, M. Savvakis, M. Hjort, D. Bliman, M. Linares, 808 C. Lindholm, E. Stavrinidou, J. Y. Gerasimov, D. T. Simon, R. Olsson and M. 809 Berggren, *Science*, 2023, **379**, 795–802. View Article Online  
DOI: 10.1039/D4NA00292J
- 810 64. Z. Zhao, H. Zhu, X. Li, L. Sun, F. He, J. E. Chung, D. F. Liu, L. Frank, L. 811 Luan and C. Xie, *Nat Biomed Eng*, 2023, **7**, 520–532.
- 812 65. K. H. Nam, M. Abdulhafez, E. Castagnola, G. N. Tomaraei, X. T. Cui and M. 813 Bedewy, *Carbon N Y*, 2022, **188**, 209–219.
- 814 66. M. E. E. Alahi, Y. Liu, S. Khademi, A. Nag, H. Wang, T. Wu and S. C. 815 Mukhopadhyay, *Biosensors (Basel)*, 2022, **12**.
- 816 67. U. J. Jeong, J. Lee, N. Chou, K. Kim, H. Shin, U. Chae, H. Y. Yu and I. J. 817 Cho, *Lab Chip*, 2021, **21**, 2383–2397.
- 818 68. Y. Tchoe, T. Wu, H. S. U, D. M. Roth, D. Kim, J. Lee, D. R. Cleary, P. 819 Pizarro, K. J. Tonsfeldt, K. Lee, P. C. Chen, A. M. Bourhis, I. Galton, B. 820 Coughlin, J. C. Yang, A. C. Paulk, E. Halgren, S. S. Cash and S. A. Dayeh, 821 *bioRxiv*, 2023, DOI: 10.1101/2023.07.19.549735.
- 822 69. M. Lee, D. Kim, H. S. Shin, H. G. Sung and J. H. Choi, *J Vis Exp*, 2011, 823 DOI: 10.3791/2562.
- 824 70. C. E. Cruttenden, J. M. Taylor, S. Hu, Y. Zhang, X. H. Zhu, W. Chen and R. 825 Rajamani, *Biomed Phys Eng Express*, 2017, **4**.
- 826 71. P. M. Rossini, S. Micera, A. Benvenuto, J. Carpaneto, G. Cavallo, L. Citi, 827 C. Cipriani, L. Denaro, V. Denaro, G. Di Pino, F. Ferreri, E. Guglielmelli, 828 K. P. Hoffmann, S. Raspopovic, J. Rigosa, L. Rossini, M. Tombini and P. 829 Dario, *Clin Neurophysiol*, 2010, **121**, 777–783.
- 830 72. M. Komatsu, E. Sugano, H. Tomita and N. Fujii, *Front Neurosci*, 2017, **11**, 831 514.
- 832 73. M. McAvoy, J. K. Tsosie, K. N. Vyas, O. F. Khan, K. Sadtler, R. Langer and 833 D. G. Anderson, *Theranostics*, 2019, **9**, 7099–7107.
- 834 74. S. H. Bae, J. H. Che, J. M. Seo, J. Jeong, E. T. Kim, S. W. Lee, K. I. Koo, 835 G. J. Suaning, N. H. Lovell, D. I. Cho, S. J. Kim and H. Chung, *Invest* 836 *Ophthalmol Vis Sci*, 2012, **53**, 2653–2657.
- 837 75. S. Srinivasan, K. Vyas, M. McAvoy, P. Calvaresi, O. F. Khan, R. Langer, D. 838 G. Anderson and H. Herr, *Front Neurol*, 2019, **10**, 252.
- 839 76. R. Herbert, S. Mishra, H. R. Lim, H. Yoo and W. H. Yeo, *Adv Sci (Weinh)*, 840 2019, **6**, 1901034.
- 841 77. B. Panda, S. Mandal and S. J. A. Majerus, *IEEE Trans Biomed Circuits Syst*, 842 2019, **13**, 1494–1505.
- 843 78. S. Nesson, M. Yu, X. Zhang and A. H. Hsieh, *J Biomed Opt*, 2008, **13**, 044040.
- 844 79. J. J. Kim, G. R. Stafford, C. Beauchamp and S. A. Kim, *Sensors (Basel)*, 845 2020, **20**.
- 846 80. H. U. Kim, H. Y. Kim, H. Seok, V. Kanade, H. Yoo, K. Y. Park, J. H. Lee, M. 847 H. Lee and T. Kim, *Anal Chem*, 2020, **92**, 6327–6333.
- 848 81. N. Radha Shanmugam, S. Muthukumar, S. Chaudhry, J. Anguiano and S. Prasad, 849 *Biosens Bioelectron*, 2017, **89**, 764–772.
- 850



- 851 82. I. Shitanda, T. Oshimoto, N. Loew, M. Motosuke, H. Watanabe, T. Mikawa and  
852 M. Itagaki, *Biosens Bioelectron*, 2023, **238**, 115555.
- 853 83. X. Xuan, H. S. Yoon and J. Y. Park, *Biosens Bioelectron*, 2018, **109**, 75–82.
- 854 84. Y. Zhu, P. Xia, J. Liu, Z. Fang, L. Du and Z. Zhao, *Micromachines (Basel)*,  
855 2022, **13**.
- 856 85. P. S. Tan, E. Vaughan, J. Islam, N. Burke, D. Iacopino and J. B. Tierney,  
857 *Nanomaterials (Basel)*, 2021, **11**.
- 858 86. J. Guo, A. E. Niaraki Asli, K. R. Williams, P. L. Lai, X. Wang, R.  
859 Montazami and N. N. Hashemi, *Biosensors (Basel)*, 2019, **9**.
- 860 87. R. Lin, Y. Jin, R. R. Li, C. Jiang, J. Ping, C. J. Charles, Y. L. Kong and  
861 J. S. Ho, *Biosens Bioelectron*, 2022, **216**, 114651.
- 862 88. Y. Tian, Y. Liu, Y. Wang, J. Xu and X. Yu, *Sensors (Basel)*, 2021, **21**.
- 863 89. Z. J. Wu, Z. Luo, A. Rastogi, S. Stavchansky, P. D. Bowman and P. S. Ho,  
864 *Biomed Microdevices*, 2011, **13**, 485–491.
- 865 90. A. Rastogi, P. D. Bowman and S. Stavchansky, *Drug Deliv Transl Res*, 2012,  
866 **2**, 106–111.
- 867 91. N. Unver, S. Odabas, G. B. Demirel and O. T. Gul, *J Mater Chem B*, 2022, **10**,  
868 8419–8431.
- 869 92. B. J. Lyon, A. I. Aria and M. Gharib, *Biomed Microdevices*, 2014, **16**, 879–  
870 886.
- 871 93. A. Santillan, D. G. Rubin, C. P. Foley, D. Sondhi, R. G. Crystal, Y. P.  
872 Gobin and D. J. Ballon, *J Neurosci Methods*, 2014, **222**, 106–110.
- 873 94. D. A. Borkholder, X. Zhu and R. D. Frisina, *J Control Release*, 2014, **174**,  
874 171–176.
- 875 95. F. Teodorescu, G. Queniat, C. Foulon, M. Lecoeur, A. Barras, S.  
876 Boulahneche, M. S. Medjam, T. Hubert, A. Abderrahmani, R. Boukherroub and  
877 S. Szunerits, *J Control Release*, 2017, **245**, 137–146.
- 878 96. Q. Pagneux, R. Ye, L. Chengnan, A. Barras, N. Hennuyer, B. Staels, D.  
879 Caina, J. I. A. Osses, A. Abderrahmani, V. Plaisance, V. Pawlowski, R.  
880 Boukherroub, S. Melinte and S. Szunerits, *Nanoscale Horiz*, 2020, **5**, 663–  
881 670.
- 882 97. S. Metz, A. Bertsch, D. Bertrand and P. Renaud, *Biosens Bioelectron*, 2004,  
883 **19**, 1309–1318.
- 884 98. Y. Hu, Y. Wang, Q. Feng, T. Chen, Z. Hao, S. Zhang, L. Cai, X. Guo and J.  
885 Li, *Biomater Sci*, 2023, **11**, 3486–3501.
- 886 99. F. S. L. Bobbert, K. Lietaert, A. A. Eftekhari, B. Pouran, S. M. Ahmadi, H.  
887 Weinans and A. A. Zadpoor, *Acta Biomater*, 2017, **53**, 572–584.
- 888 100. A. J. T. Teo, A. Mishra, I. Park, Y. J. Kim, W. T. Park and Y. J. Yoon, *ACS*  
889 *Biomater Sci Eng*, 2016, **2**, 454–472.
- 890 101. R. Kaewmanee, F. Wang, Y. Pan, S. Mei, J. Meesane, F. Li, Z. Wu and J. Wei,  
891 *Biomater Sci*, 2022, **10**, 4243–4256.
- 892 102. S. Asadullah, S. Mei, K. Yang, X. Hu, F. Wang, B. Yu, Z. Wu and J. Wei, *J*  
893 *Mech Behav Biomed Mater*, 2021, **124**, 104800.





- 894 103. Y. Zhang, W. Jiang, S. Yuan, Q. Zhao, Z. Liu and W. Yu, *Int J Nanomedicine*, 2020, **15**, 9389–9405. View Article Online  
DOI: 10.1039/D4NA00292J
- 895
- 896 104. Y. Ling, W. Pang, J. Liu, M. Page, Y. Xu, G. Zhao, D. Stalla, J. Xie, Y. Zhang and Z. Yan, *Nat Commun*, 2022, **13**, 524.
- 897
- 898 105. N. El-Atab, N. Qaiser, H. Badghaish, S. F. Shaikh and M. M. Hussain, *ACS Nano*, 2020, **14**, 7659–7665.
- 899
- 900 106. M. Loeb, A. Bartholomew, M. Hashmi, W. Tarhuni, M. Hassany, I. Youngster, R. Somayaji, O. Larios, J. Kim, B. Missaghi, J. V. Vayalunkal, D. Mertz, Z. Chagla, M. Cividino, K. Ali, S. Mansour, L. A. Castellucci, C. Frenette, L. Parkes, M. Downing, M. Muller, V. Glavin, J. Newton, R. Hookoom, J. A. Leis, J. Kinross, S. Smith, S. Borhan, P. Singh, E. Pullenayegum and J. Conly, *Ann Intern Med*, 2022, **175**, 1629–1638.
- 901
- 902
- 903
- 904
- 905
- 906 107. F. Topuz, M. A. Abdulhamid, R. Hardian, T. Holtzl and G. Szekely, *J Hazard Mater*, 2022, **424**, 127347.
- 907
- 908 108. H. W. Chen, Y. L. Kuo, C. H. Chen, C. S. Chiou, W. T. Chen and Y. H. Lai, *Process Saf Environ Prot*, 2022, **167**, 695–707.
- 909
- 910 109. H. Zhong, Z. Zhu, P. You, J. Lin, C. F. Cheung, V. L. Lu, F. Yan, C. Y. Chan and G. Li, *ACS Nano*, 2020, **14**, 8846–8854.
- 911
- 912 110. B. Ghatak, S. Banerjee, S. B. Ali, R. Bandyopadhyay, N. Das, D. Mandal and B. Tudu, *Nano Energy*, 2021, **79**, 105387.
- 913
- 914 111. R. Kaewmanee, F. Wang, S. Mei, Y. Pan, B. Yu, Z. Wu, J. Meesane and J. Wei, *J Mater Chem B*, 2022, **10**, 5058–5070.
- 915
- 916 112. W. Ma, Y. Li, M. Zhang, S. Gao, J. Cui, C. Huang and G. Fu, *ACS Appl Mater Interfaces*, 2020, **12**, 34999–35010.
- 917
- 918 113. E. A. Cuello, L. E. Mulko, C. A. Barbero, D. F. Acevedo and E. I. Yslas, *Colloids Surf B Biointerfaces*, 2020, **188**, 110801.
- 919
- 920 114. D. U. Lee, D. W. Kim, S. Y. Lee, D. Y. Choi, S. Y. Choi, K. S. Moon, M. Y. Shon and M. J. Moon, *Colloids Surf B Biointerfaces*, 2022, **211**, 112314.
- 921
- 922 115. Q. Li, J. Li, G. Liao and Z. Xu, *J Mater Sci Mater Med*, 2018, **29**, 126.
- 923
- 924 116. R. Eivazzadeh-Keihan, Z. Sadat, A. Mohammadi, H. Aghamirza Moghim Aliabadi, A. Kashtiaray, A. Maleki and M. Mahdavi, *Sci Rep*, 2023, **13**, 9598.
- 925
- 926 117. M. Mariello, A. Qualtieri, G. Mele and M. De Vittorio, *ACS Appl Mater Interfaces*, 2021, **13**, 20606–20621.
- 927
- 928 118. T. K. Nguyen, M. Barton, A. Ashok, T. A. Truong, S. Yadav, M. Leitch, T. V. Nguyen, N. Kashaninejad, T. Dinh, L. Hold, Y. Yamauchi, N. T. Nguyen and H. P. Phan, *Proc Natl Acad Sci U S A*, 2022, **119**, e2203287119.
- 929
- 930



931 **Figure legends**

932 **Fig. 1. Different forms of PI for different applications.** PIs were prepared  
933 as fibers, films, foams, resins, electronic substrates, and liquids for  
934 analysis in different applications.

935 **Fig. 2. Schematic representations of the synthesis of PI.**

936 **(A)** Synthesis of aromatic polyimides based on unsymmetrical diamine 3,4'-  
937 ODA and various tetracarboxylic acid dianhydrides. Reproduced with  
938 permission<sup>24</sup>. Copyright 2022, MDPI. **(B)** Preparation of HSHMPI fibers  
939 through an integrated continuous wet-spinning method. Reproduced with  
940 permission<sup>22</sup>. Copyright 2018, WILEY-VCH. **(C)** Synthesis of a BPDA-PDA  
941 polyimide. Reproduced with permission<sup>25</sup>. Copyright 2020, MDPI. **(D)** The  
942 electrospinning process. Reproduced with permission<sup>26</sup>. Copyright 2022,  
943 MDPI. **(E)** Synthesis of polyimide R-BAPBs with different molecular weights.  
944 Reproduced with permission<sup>27</sup>. Copyright 2023, MDPI. **(F)** Synthesis of a  
945 BPADA-ODA PI. Reproduced with permission<sup>28</sup>. Copyright 2015, Nature  
946 Publishing Group. **(G)** Synthesis of bismaleimide resin modified with  
947 hyperbranched polyimide. Reproduced with permission<sup>29</sup>. Copyright 2022,  
948 MDPI. **(H)** Synthesis of a 6FDA/ODPA-ODA polyimide. Reproduced with  
949 permission<sup>30</sup>. Copyright 2021, MDPI. **(I)** The preparation of 3FPODA and  
950 synthesis of copolymerized polyimide. Reproduced with permission<sup>32</sup>.  
951 Copyright 2022, MDPI. **(J)** Synthesis of an organosoluble Fluoro-containing  
952 polyimide. Reproduced with permission<sup>33</sup>. Copyright 2022, MDPI.

953 **Fig. 3. Stability tests for PI.** **(A)** TGA thermograms for neat polyimide,  
954 graphene, and Cloisite 30B clay in a nitrogen atmosphere at a heating rate  
955 of 30°C/min. Reproduced with permission<sup>36</sup>. Copyright 2021, MDPI. **(B)**  
956 The tensile strength and Young's modulus of a PI-Mica film changed little  
957 after AO, UV, and high-temperature exposure. Reproduced with  
958 permission<sup>37</sup>. Copyright 2013, WILEY-VCH.

959 **(C~E)** The mass loss curve (C) and stress-strain curve (D, E) of PI stored  
960 in PBS showed that PI was stable in PBS at body temperature and even at



961 60°C. Reproduced with permission<sup>38</sup>. Copyright 2010, Elsevier. **(F-H)**  
962 Electrochemical impedance spectroscopy (F) and long-term imaging (G) of  
963 a PI probe implanted in the mouse cortex for 180 d. SEM image showing  
964 the overall intact probe and no signs of delamination or corrosion (H).  
965 Reproduced with permission<sup>40</sup>. Copyright 2023, WILEY-VCH. SEM of a  
966 microelectrode six months after implantation in rabbit eyes without  
967 damage to the surface or accumulation of tissue matter. Reproduced with  
968 permission<sup>15</sup>. Copyright 2013, Springer Nature.

969 **Fig. 4. Biocompatibility tests for PI.** **(A)** Rabbit retina layer six months after  
970 PI electrode implantation (upper) and control retina implantation (lower).  
971 Reproduced with permission<sup>15</sup>. Copyright 2013, Springer Nature. **(B)**  
972 Images of endothelial cells subjected to direct contact cytotoxicity  
973 microscopy. (a) Untreated control. (b) Methanol-treated positive control.  
974 (c) HDPE, negative material control. (d) Latex, positive material control.  
975 (e) PI. Reproduced with permission<sup>55</sup>. Copyright 2013, WILEY-VCH. **(C,**  
976 **D)** Hemocompatibility tests. The spreading of blood proteins (C), red  
977 blood cells, and platelets (D) over the surface of the poly(EPICLON-PPD)  
978 and Kapton (PI) films. Reproduced with permission<sup>57</sup>. Copyright 2016,  
979 Springer Nature. **(E)** The immune system responses to a PI electrode (a~d)  
980 implanted for 28 days in the sheep brain were minimal compared with  
981 those to the negative control material (e~h). These effects were evaluated  
982 via the accumulation of immune system cells, necrosis,  
983 neovascularization, fibrosis, and astrocytosis/fatty infiltration.  
984 Reproduced with permission<sup>61</sup>. Copyright 2022, Aura Kullmann. **(F)** Long-  
985 term safety study. PI material (CyPass) implantation increases endothelial  
986 cell loss over time in patients with cataracts. Reproduced with permission  
987 <sup>62</sup>. Copyright 2019, Elsevier.

988 **Fig. 5. PI electrodes in the nervous system.** **(A)** Schematic illustration of  
989 flexible nanomembranes wrapped around a sciatic nerve for long-term  
990 application of electrical stimuli and sensing. Reproduced with permission



991 <sup>118</sup>. Copyright 2022, PNAS. **(B)** Thin-film intracortical multilayer array  
992 probe, which is robust and flexible. Reproduced with permission <sup>40</sup>.  
993 Copyright 2023, WILEY-VCH. **(C)** 3D representation of depth probes  
994 within the brain cortex of a rat. Reproduced with permission <sup>42</sup>. Copyright  
995 2022, Elsevier. **(D)** Subdural electrocorticography (ECoG) electrode arrays  
996 were positioned through a small window through the skull of the rat's brain.  
997 Reproduced with permission <sup>67</sup>. Copyright 2021, Royal Society of  
998 Chemistry. **(E)** A stimulating thin-film microelectrode array was implanted  
999 on the surface of a rabbit retina. Reproduced with permission <sup>15</sup>. Copyright  
1000 2013, Springer Nature. **(F, G)** The rat sciatic nerve (F) and the median  
1001 human nerve (G) were transversally implanted with a transverse  
1002 intrafascicular multichannel electrode (TIME) device. Reproduced with  
1003 permission<sup>43</sup>. Copyright 2010, Elsevier.

1004 **Fig. 6. Different applications of PI-based biosensors.**

1005 **(A)** Implantable batteryless biosensor for real-time monitoring of cerebral  
1006 aneurysm hemodynamics. Reproduced with permission <sup>76</sup>. Copyright 2019,  
1007 WILEY-VCH. **(B)** Flexible sensor array for dialysis vascular access  
1008 monitoring (recording and processing blood flow sounds to determine  
1009 stenosis risk). Reproduced with permission <sup>77</sup>. Copyright 2019, MDPI. **(C)**  
1010 Integrated strain sensing platform for high-throughput drug toxicity  
1011 screening. Reproduced with permission<sup>16</sup>. Copyright 2021, Elsevier. **(D)**  
1012 Miniature pressure sensor for the intradiscal pressure measurements.  
1013 Reproduced with permission <sup>78</sup>. Copyright 2008, SPIE **(E)** A temperature  
1014 sensor adheres around an abutment wing of the dental implant platform.  
1015 Reproduced with permission <sup>79</sup>. Copyright 2020, MDPI. **(F)** Wearable sweat-  
1016 based glucose biosensor. Reproduced with permission<sup>83</sup>. Copyright 2018,  
1017 Elsevier. **(G)** Film bulk acoustic resonator humidity sensor. Reproduced  
1018 with permission <sup>84</sup>. Copyright 2022, MDPI. **(H)** Microsensor array  
1019 mounted on a 1.25 mm diameter needle for early detection of



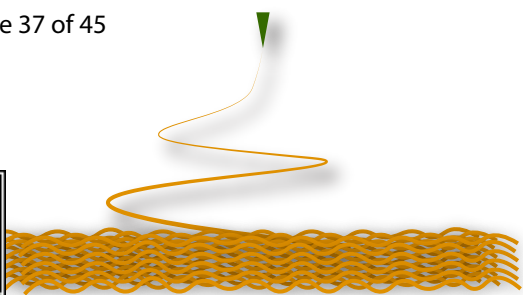
1020 extravasation in intravenous therapy. Reproduced with permission <sup>87</sup>.  
1021 Copyright 2022, Elsevier.

1022 **Fig. 7. PIs in drug delivery systems. (A)** Perforated PI tube for subcutaneous  
1023 implantation. Reproduced with permission <sup>90</sup>. Copyright 2012, Springer US.  
1024 **(B)** Hollow MN array for transdermal drug delivery. Reproduced with permission  
1025 <sup>91</sup>. Copyright 2022, Royal Society of Chemistry. **(C)** PI microcatheters for  
1026 intra-arterial delivery. Reproduced with permission <sup>93</sup>. Copyright 2013,  
1027 Elsevier. **(D)** Structural representations of 3D porous PI covalent organic  
1028 frameworks. Reproduced with permission <sup>50</sup>. Copyright 2020, ACS. **(E)**  
1029 Electrothermal patches with PI substrates. Reproduced with permission <sup>96</sup>.  
1030 Copyright 2020, Royal Society of Chemistry. **(F)** Illustration of an implantable,  
1031 flexible PI probe with microelectrodes and microfluidic channels. Reproduced with  
1032 permission<sup>97</sup>. Copyright 2004, Elsevier.

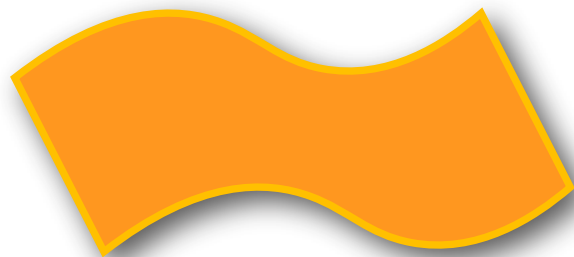
1033 **Fig. 8. SME images of different polyimide-based composites for bone**  
1034 **replacement. (A-C)** Flower-like molybdenum disulfide (fMD)-PI composites with  
1035 0%, 5 wt% and 10 wt% fMD contents. **(D-F)** A-C under different magnifications.  
1036 Reproduced with permission<sup>101</sup>. Copyright 2022, Royal Society of  
1037 Chemistry. **(G-I)** Tantalum oxide (vTO)-PI composites (PISTs) with 0%, 10%, and  
1038 15% vTO contents. **(J-L)** G-I under different magnifications. Reproduced with  
1039 permission<sup>102</sup>. Copyright 2021, Elsevier. **(M-O)** Nanolaponite ceramic (LC)-PI  
1040 composites (LPCs) with 0%, 20 wt% and 40 wt% LC content. **(P-R)** M-O under  
1041 different magnifications. Reproduced with permission <sup>103</sup>. Copyright 2020,  
1042 DOVE.

1043 **Fig. 9. Different types of PIs were synthesized to analyze their**  
1044 **antibacterial properties.** The different forms of PI were prepared as  
1045 films, patches, fibers, fabrics, and gauze.

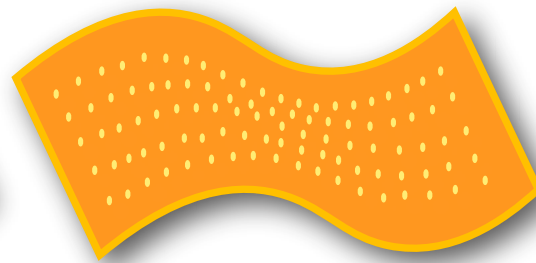




Electrospun Fiber



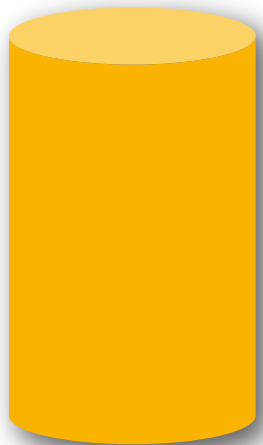
Film



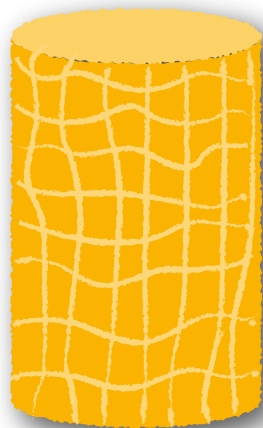
Porous Film



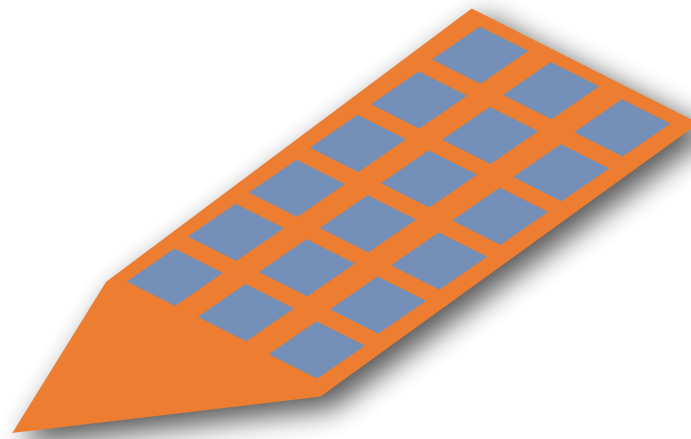
Foam



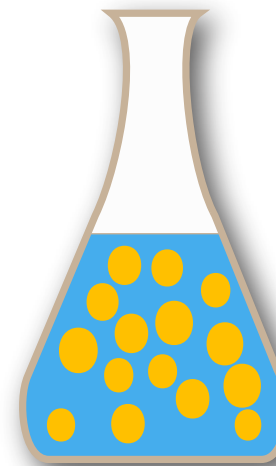
Smooth Resin



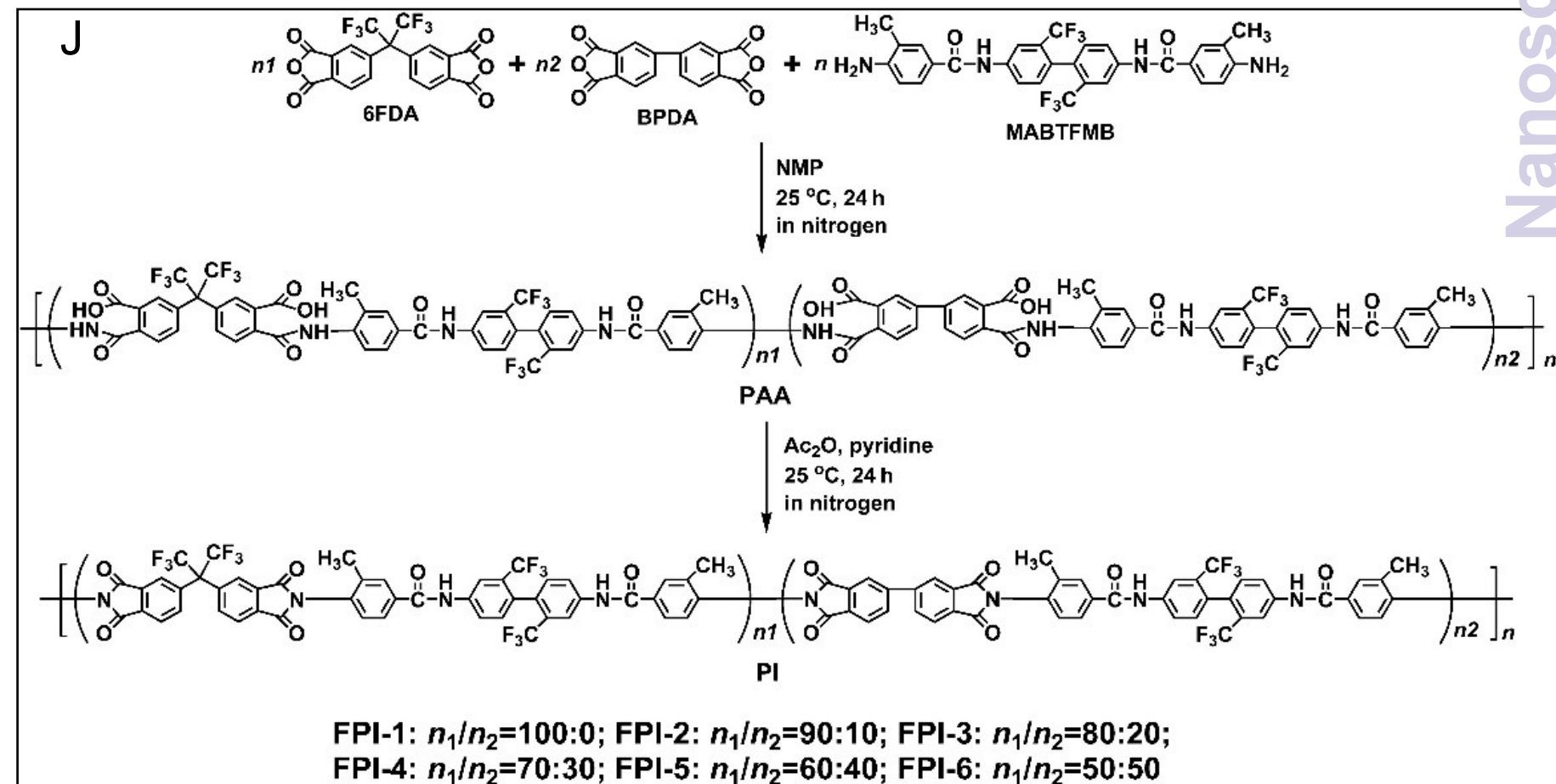
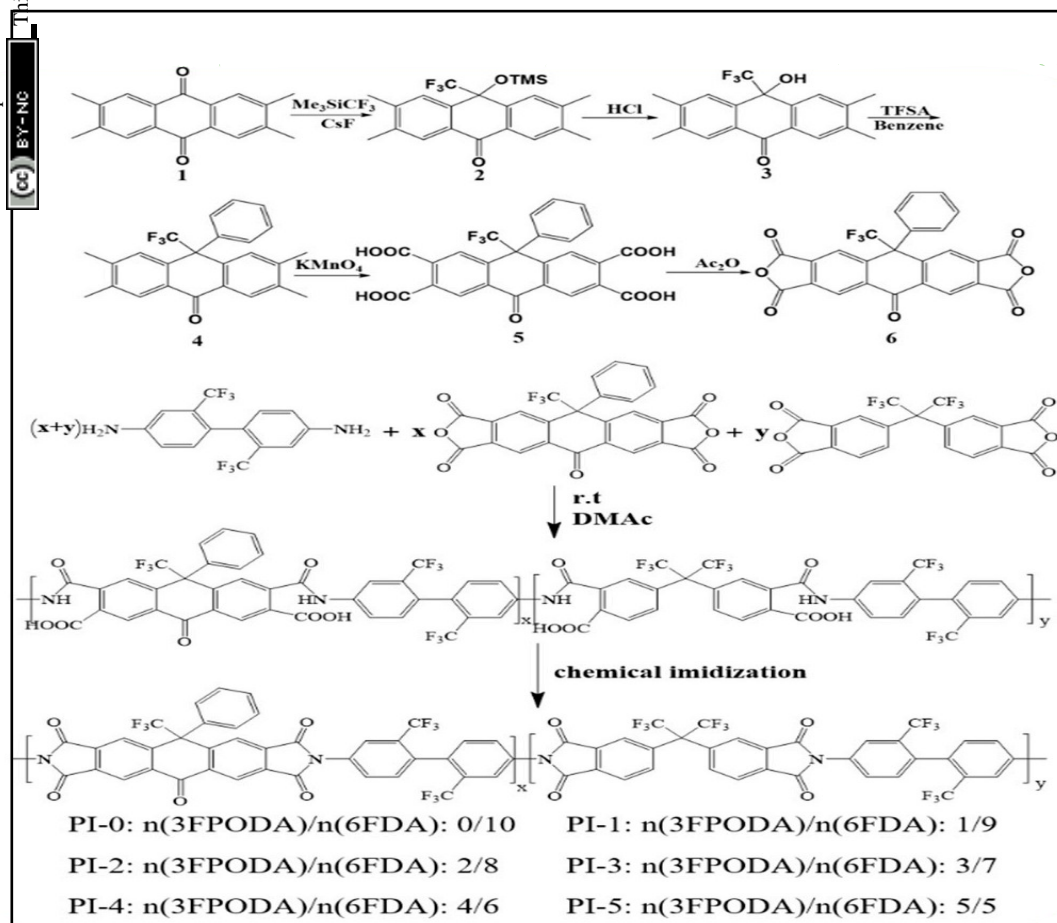
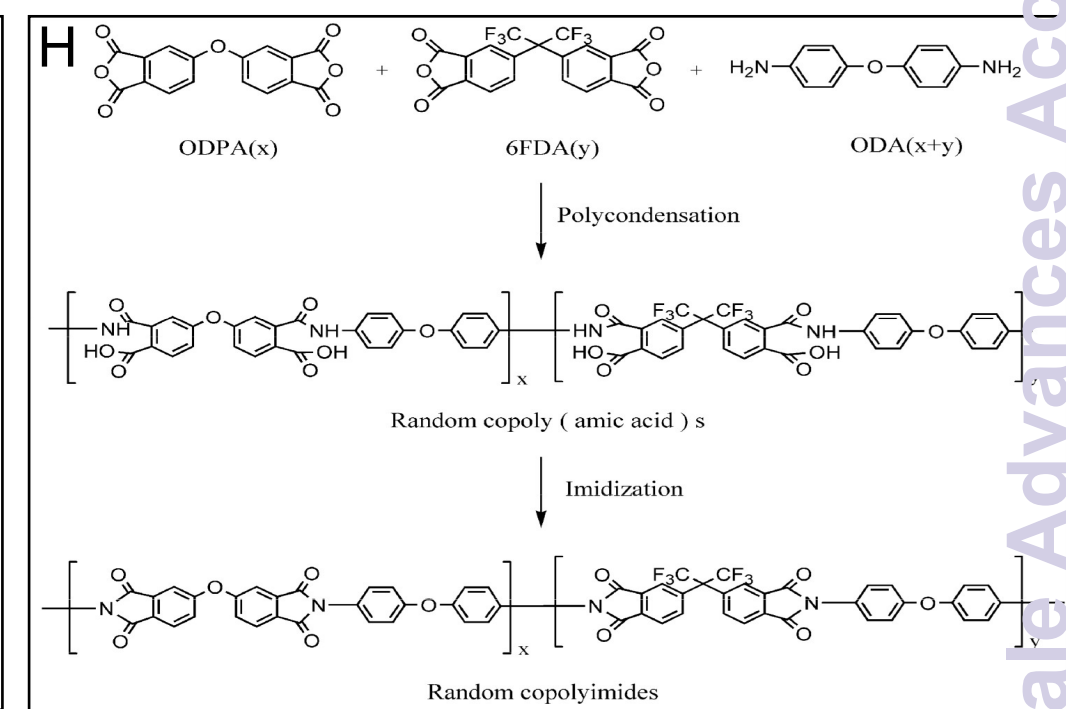
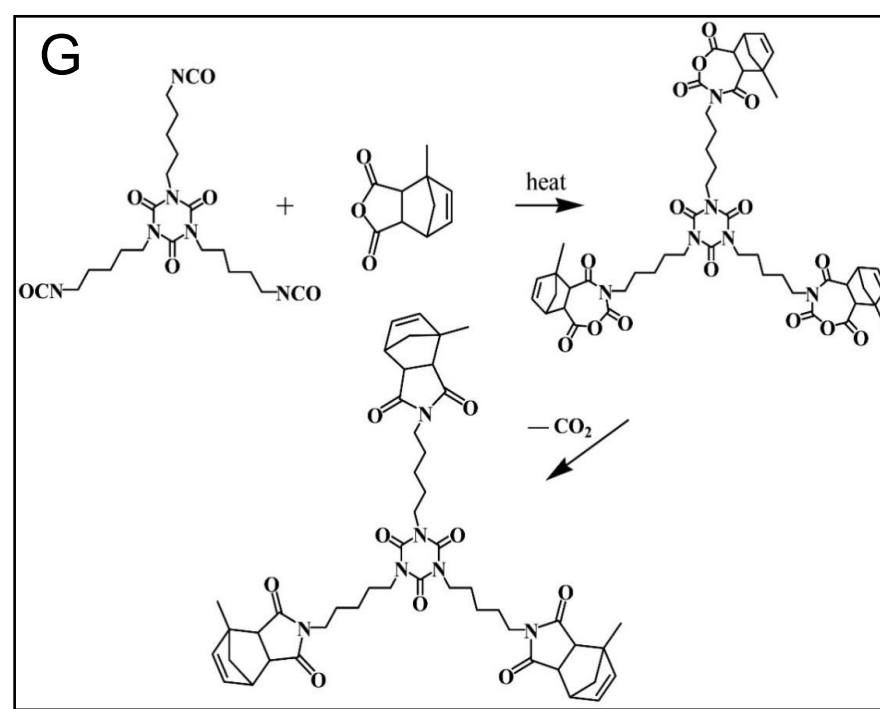
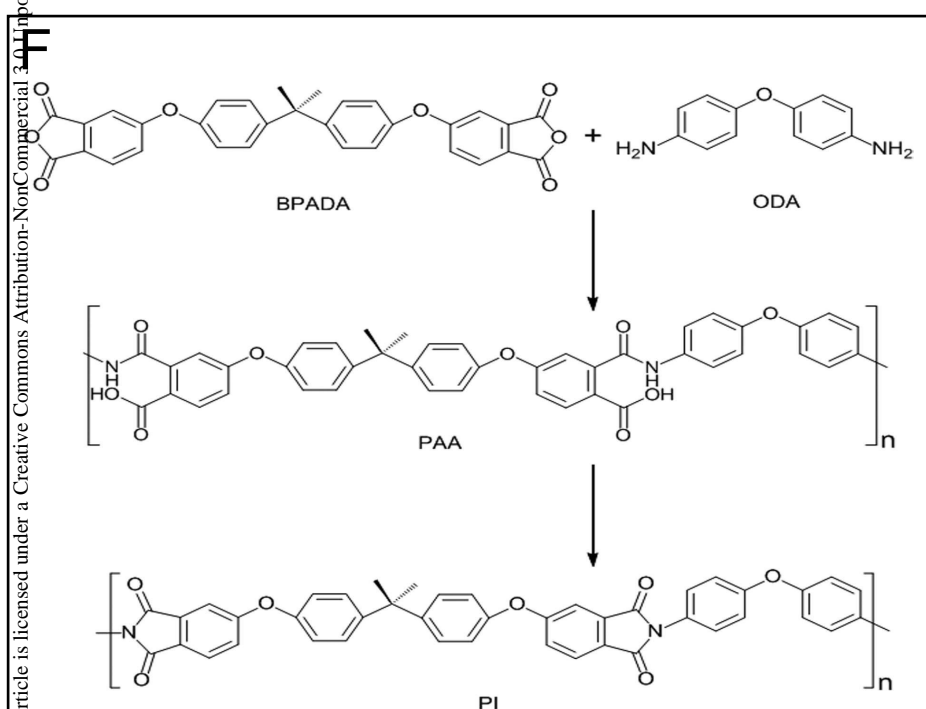
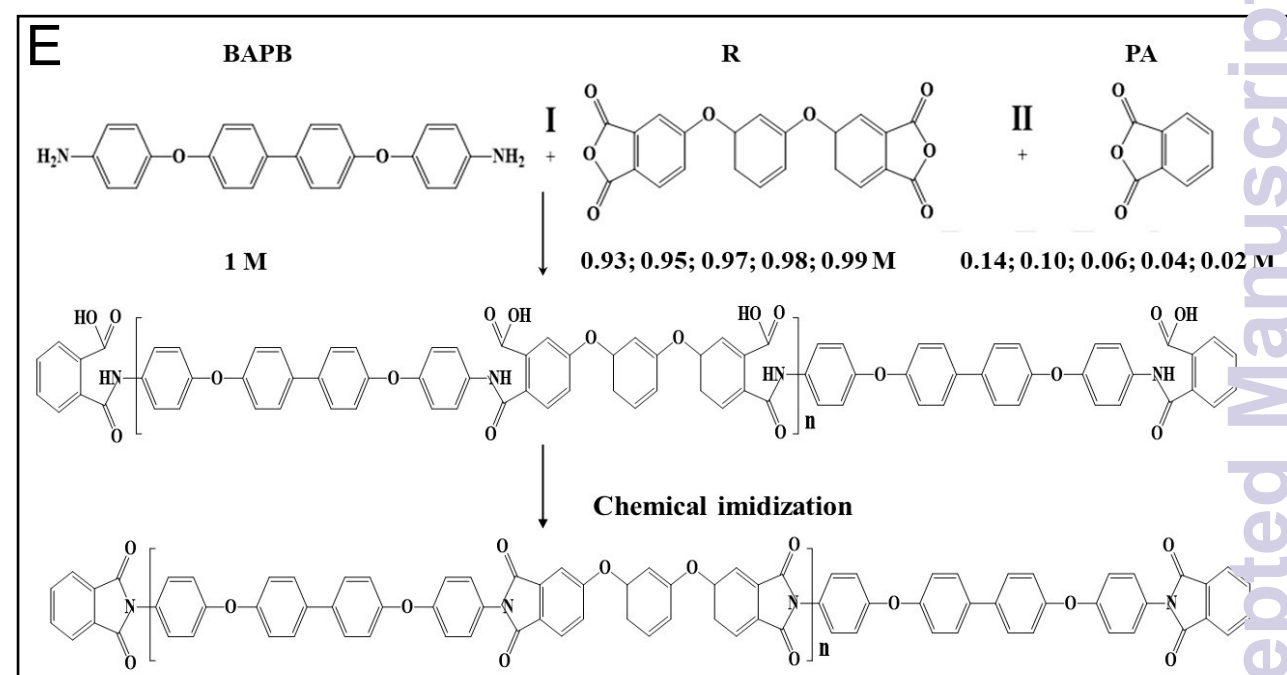
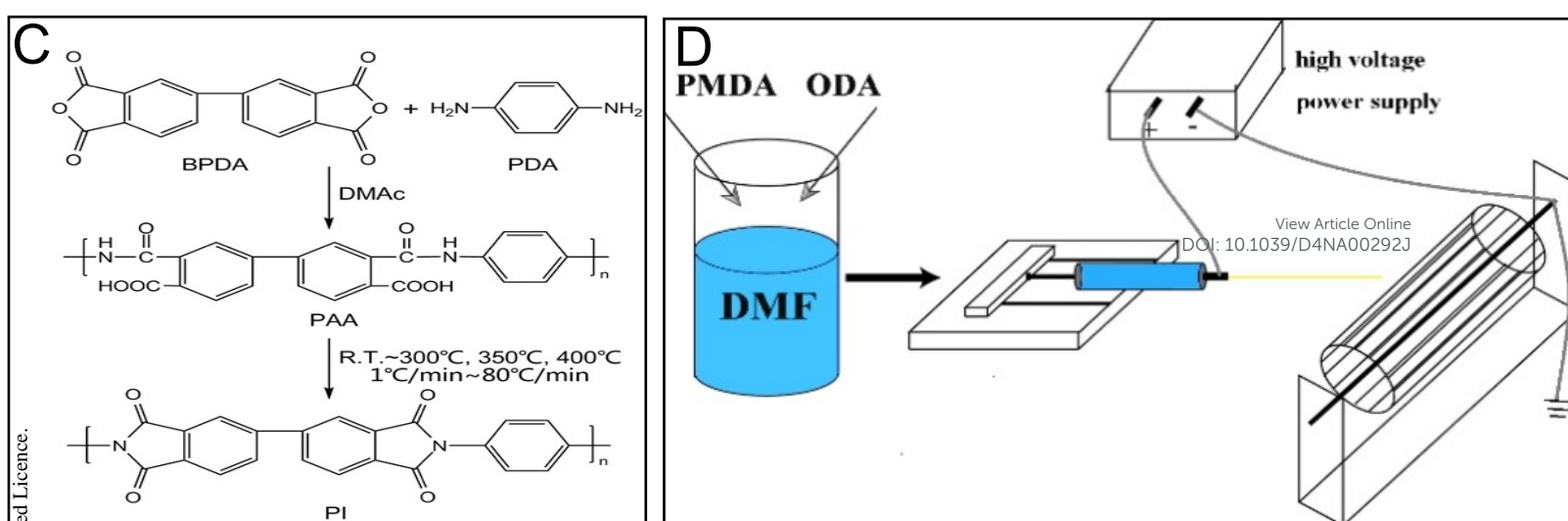
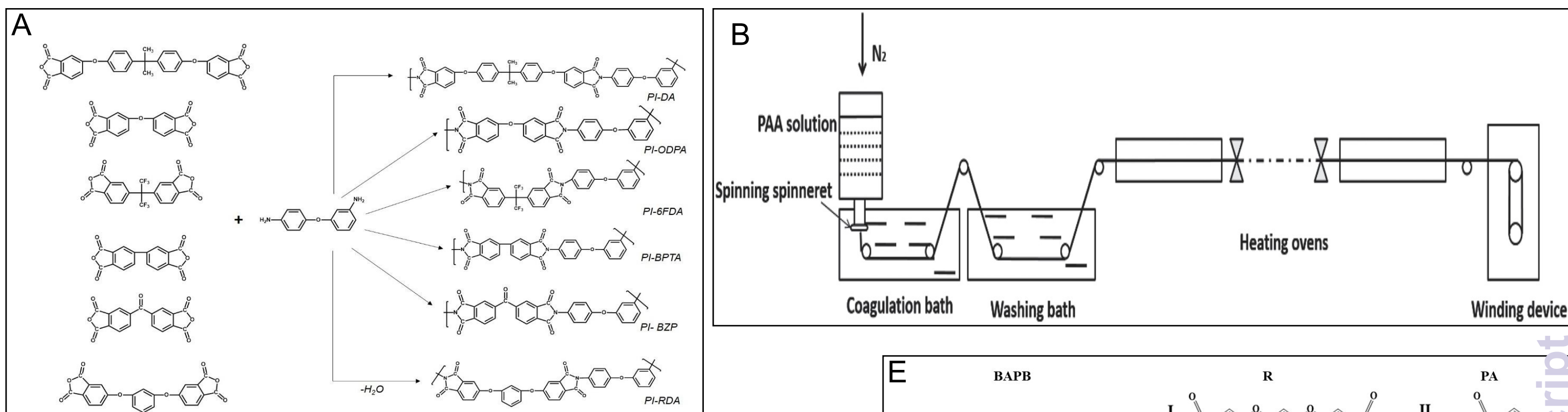
Rough Resin



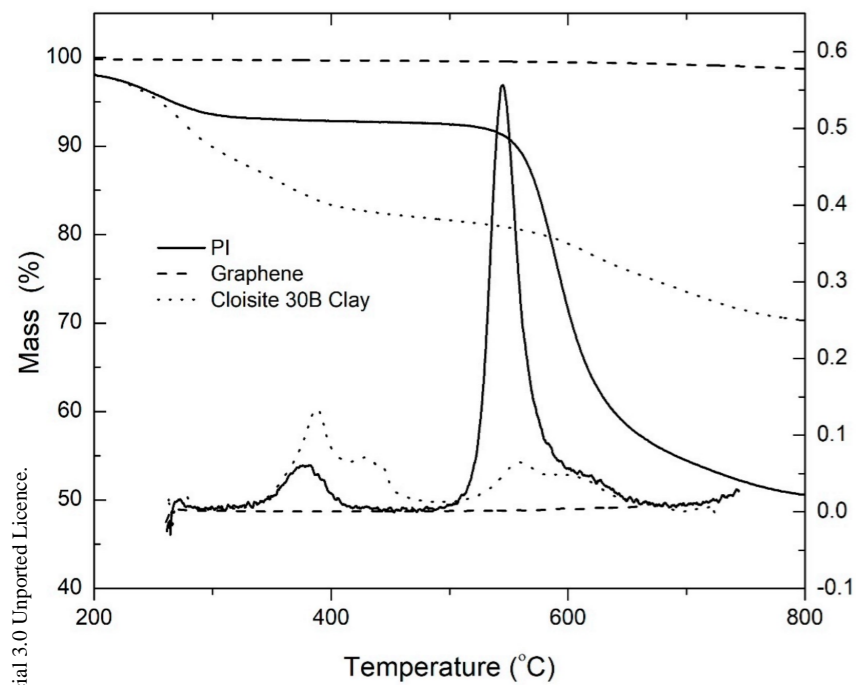
Flexible Electronic Substrate



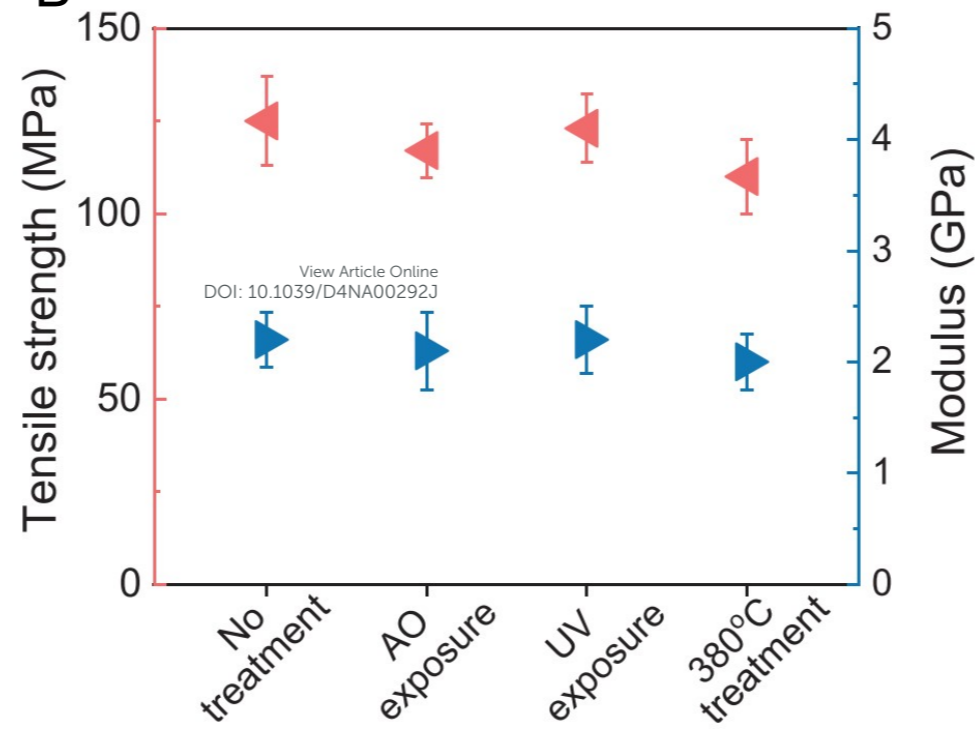
Soluble PI



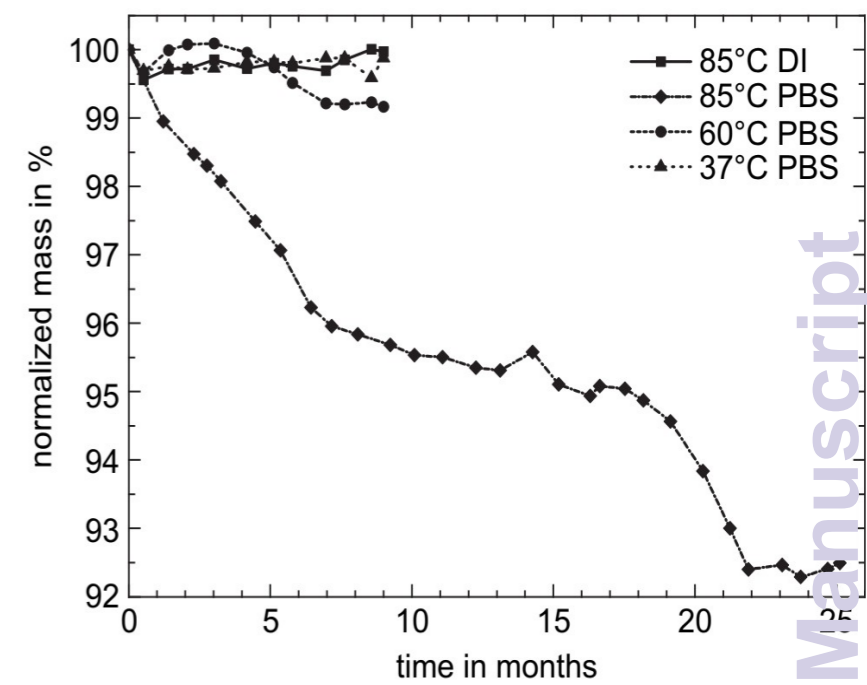
A



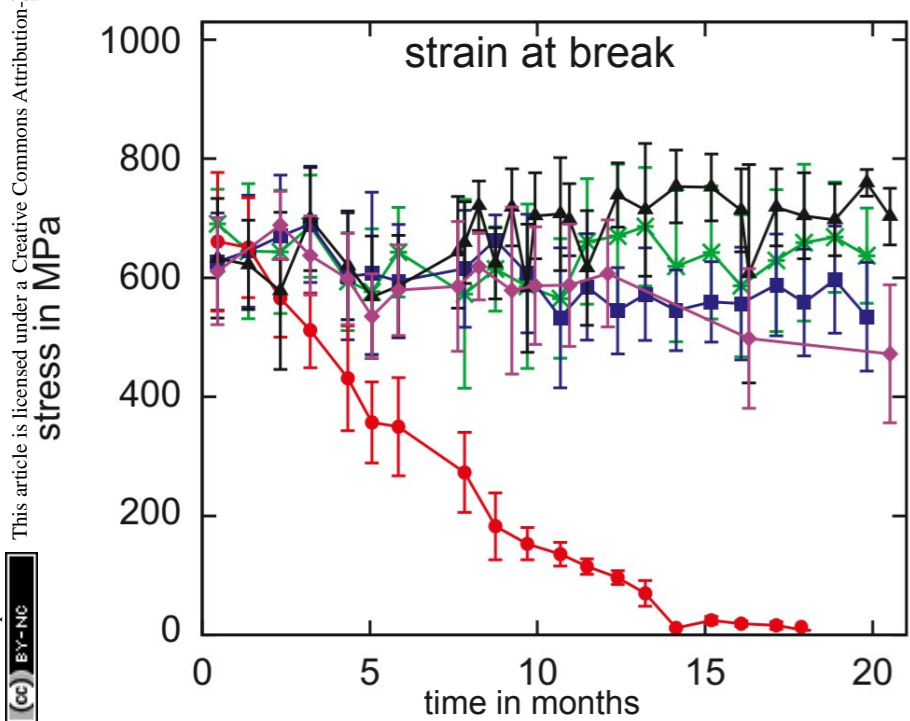
B



C

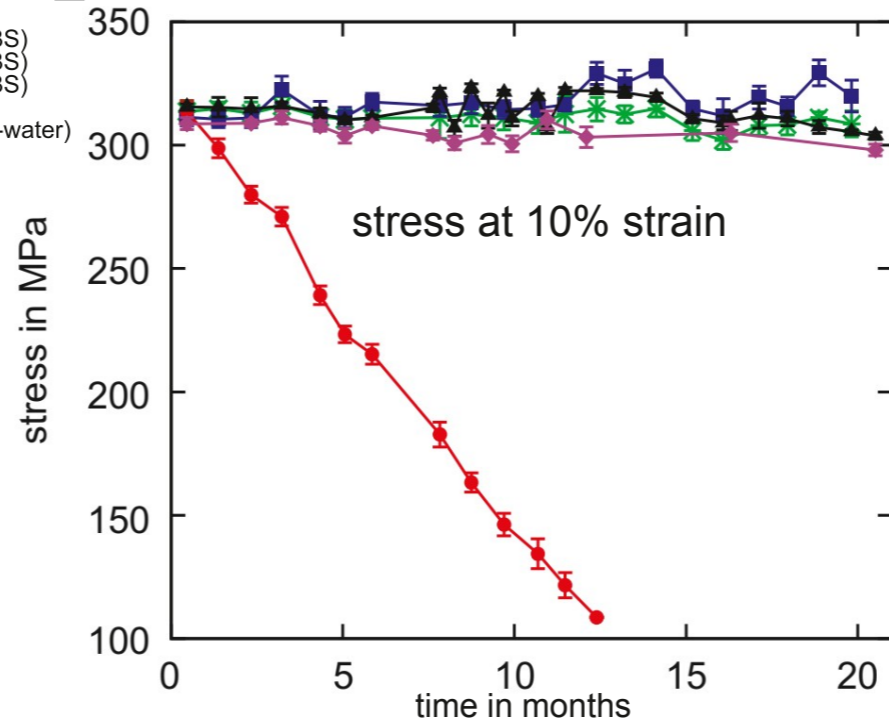


D

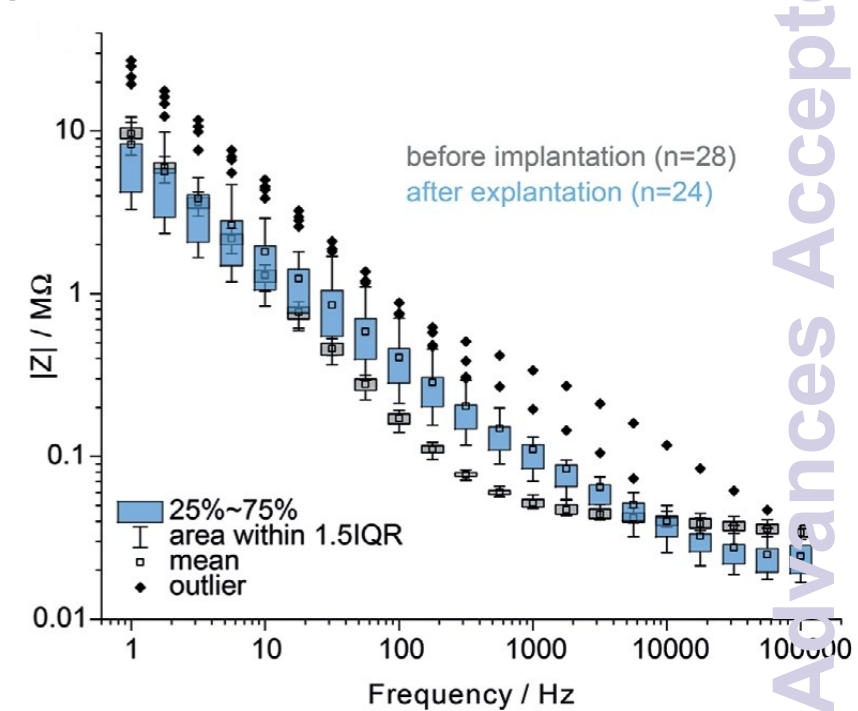


—\*— 37 °C (PBS)  
—■— 60 °C (PBS)  
—●— 85 °C (PBS)  
—▲— reference  
—◆— 85 °C (DI-water)

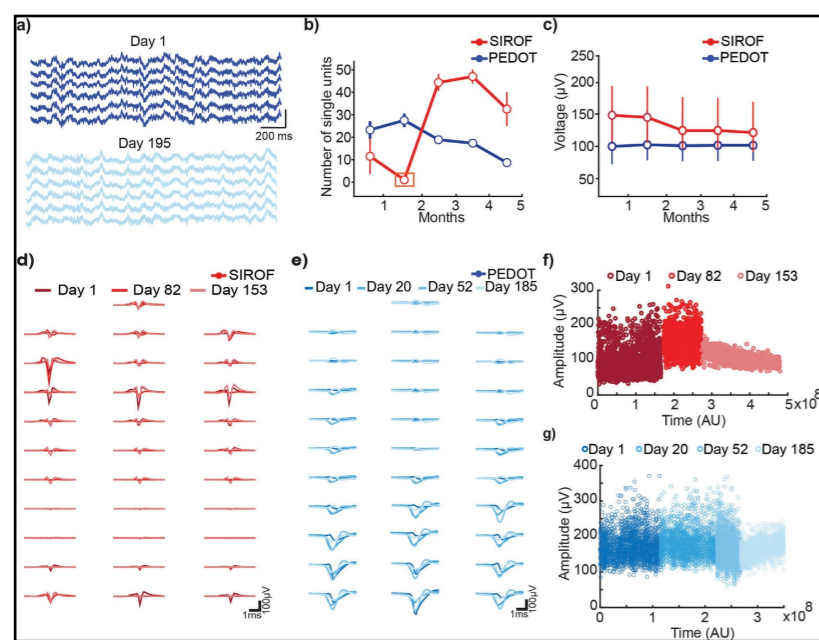
E



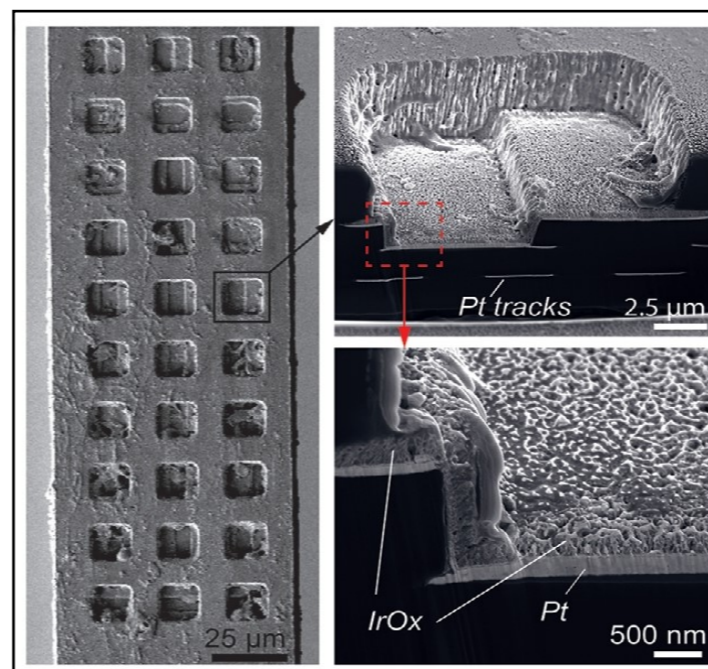
F



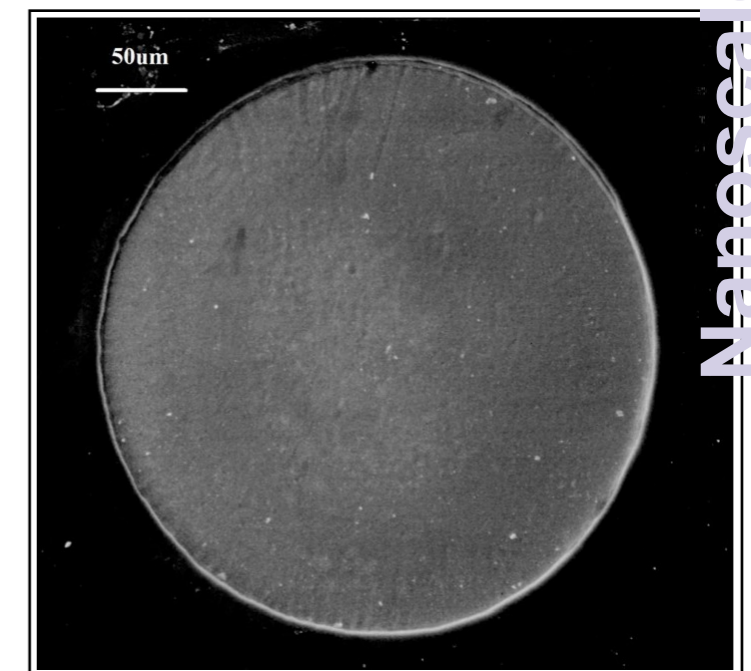
G



H



I

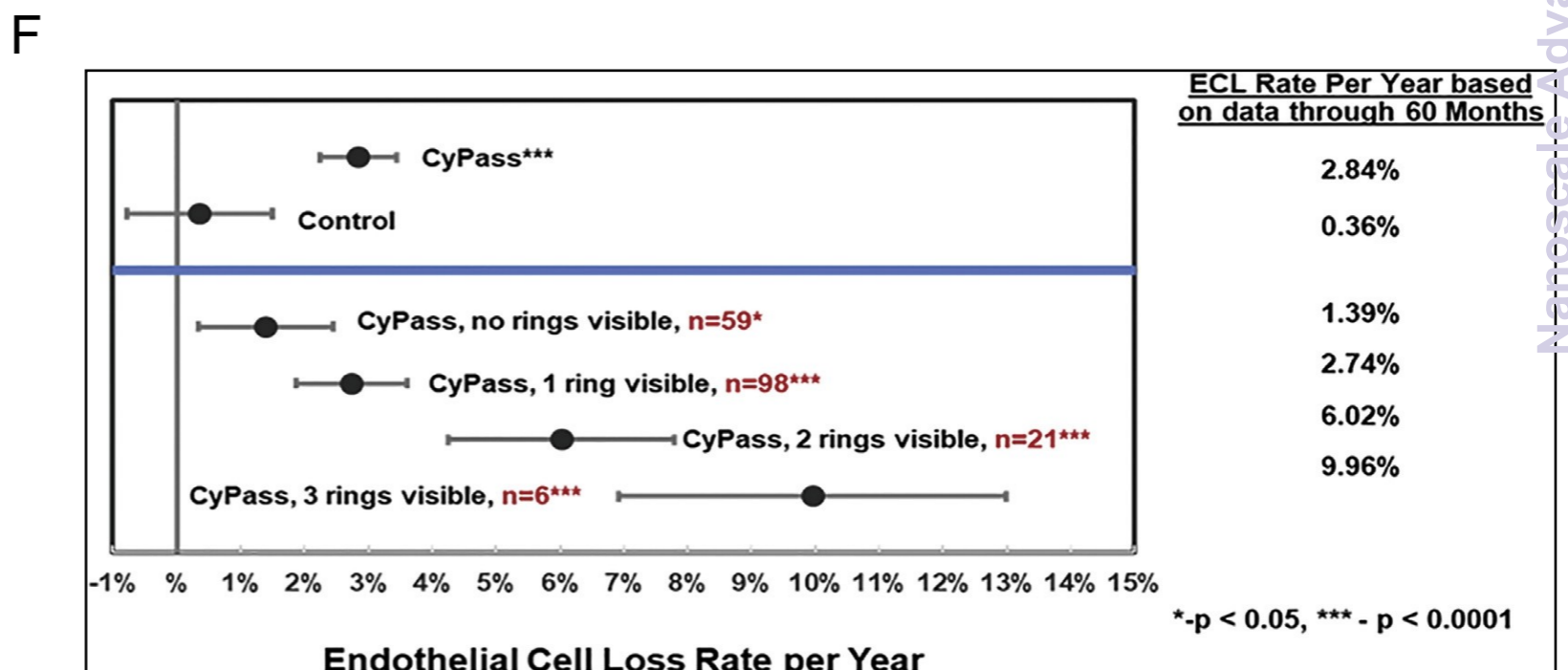
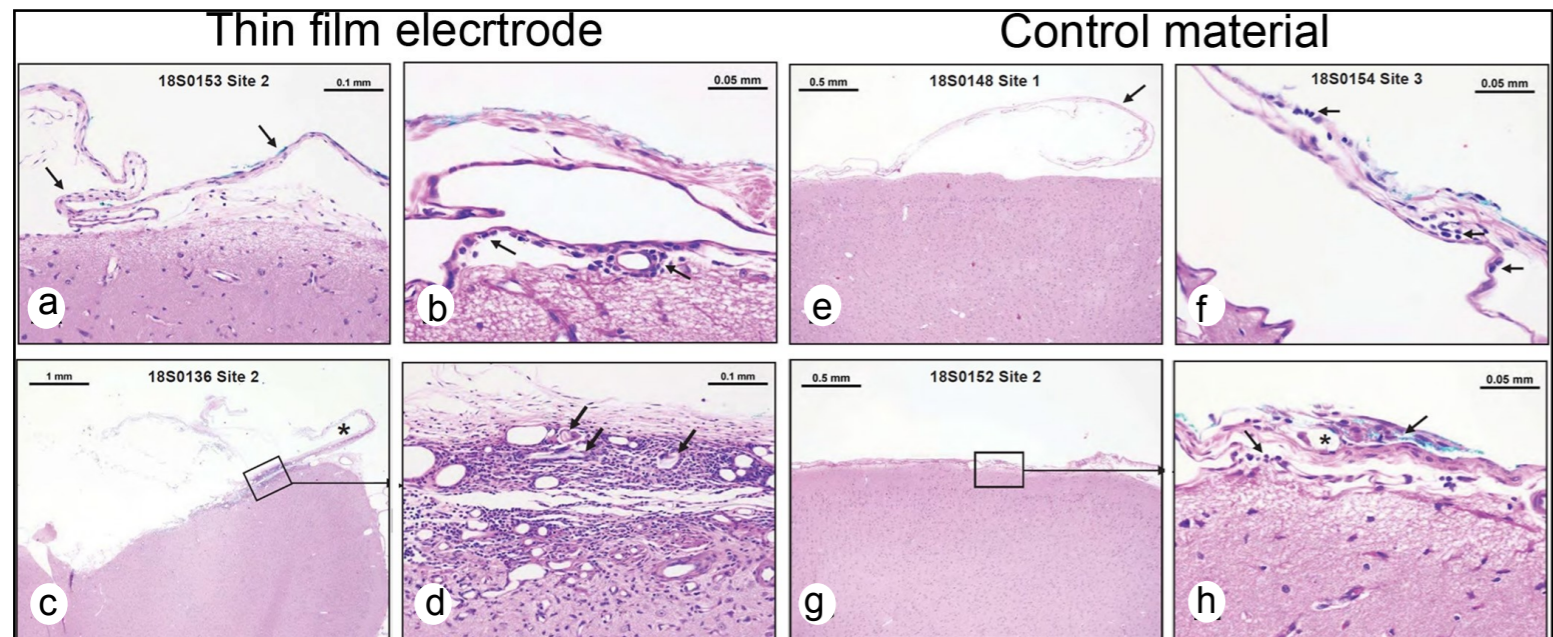
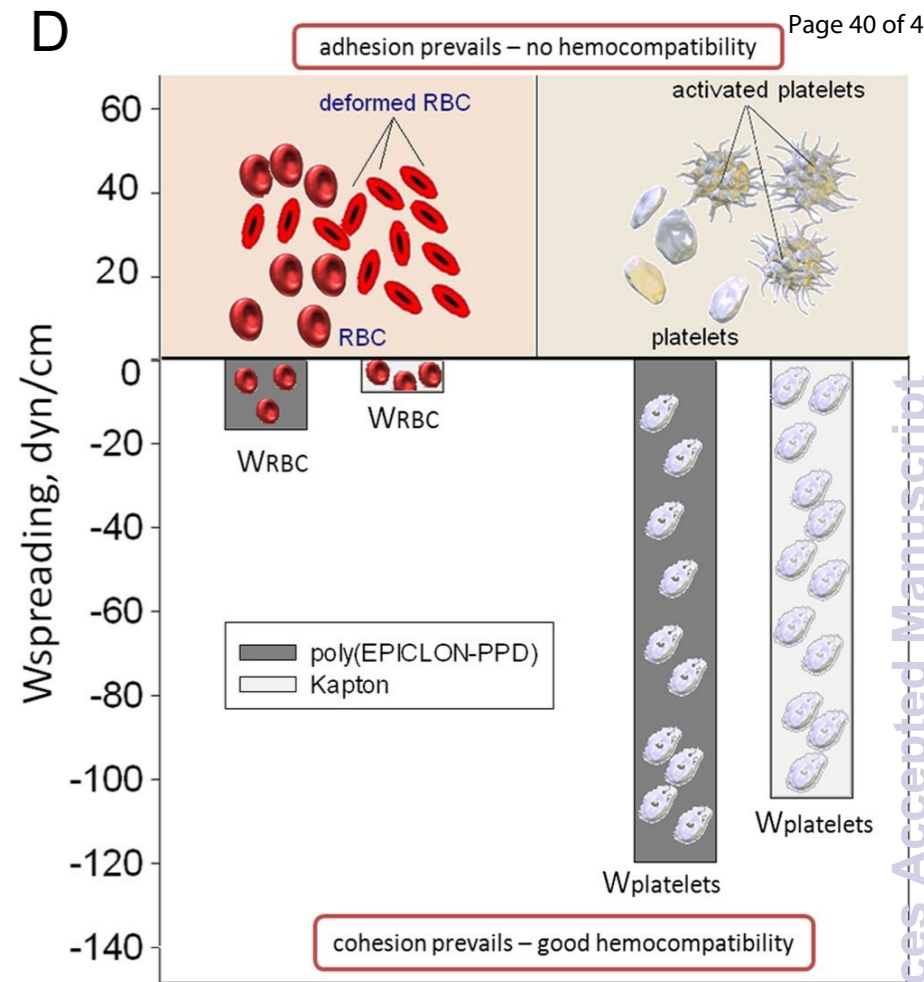
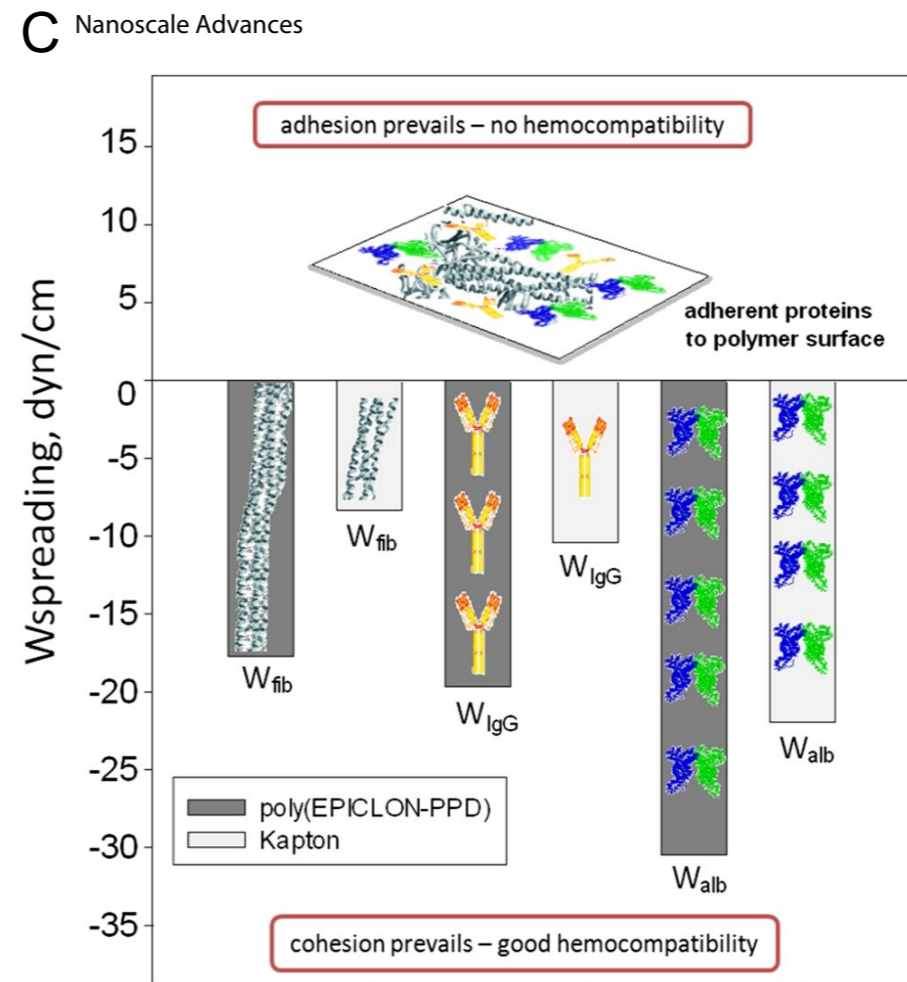
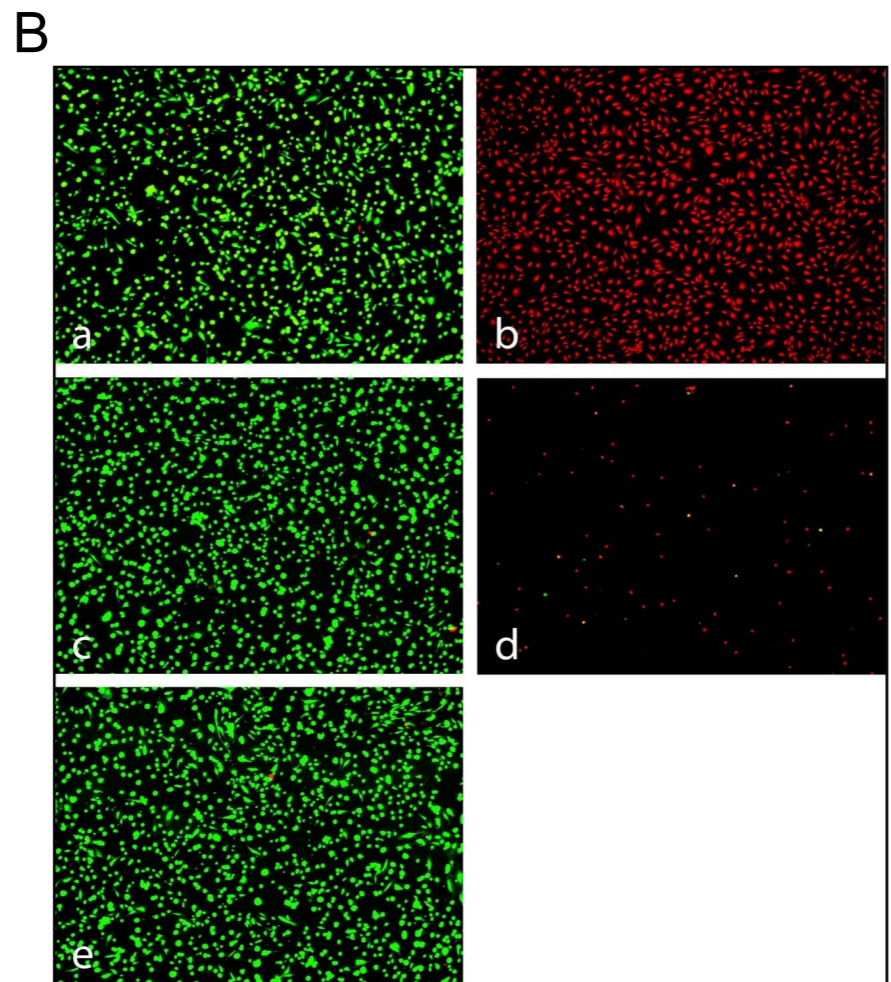
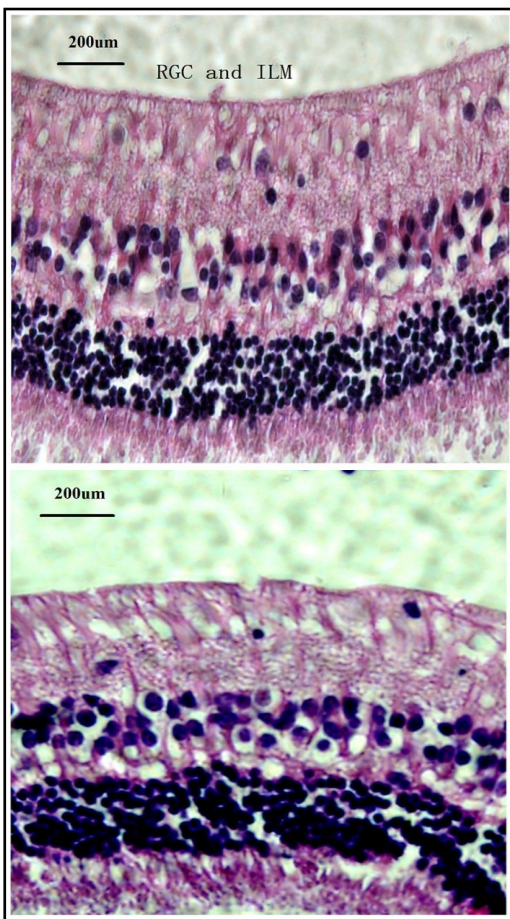


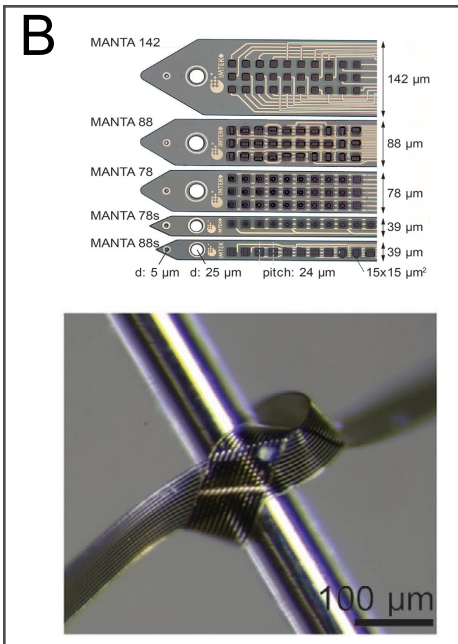
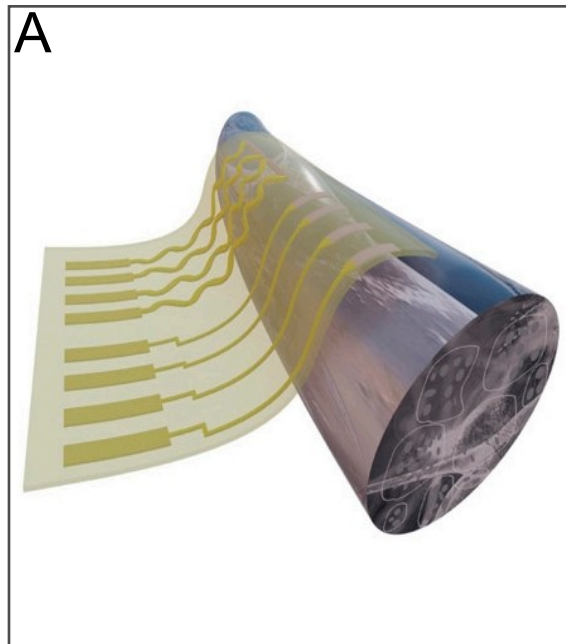




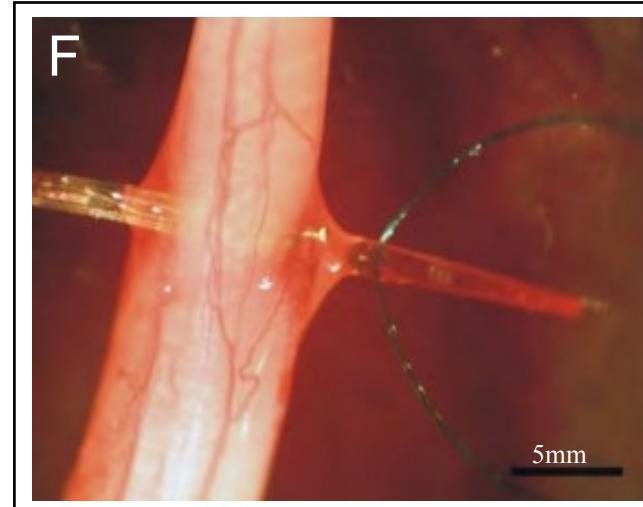
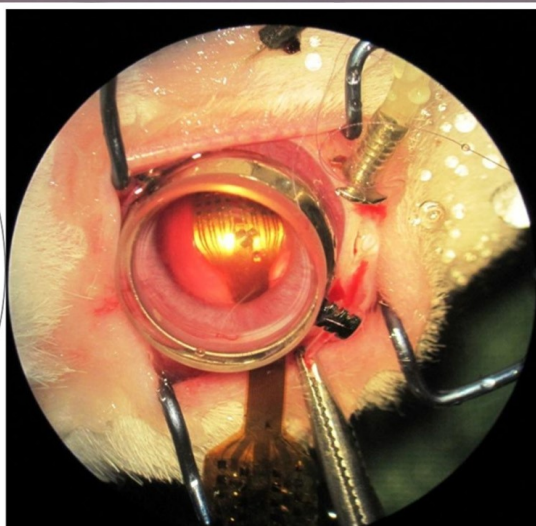
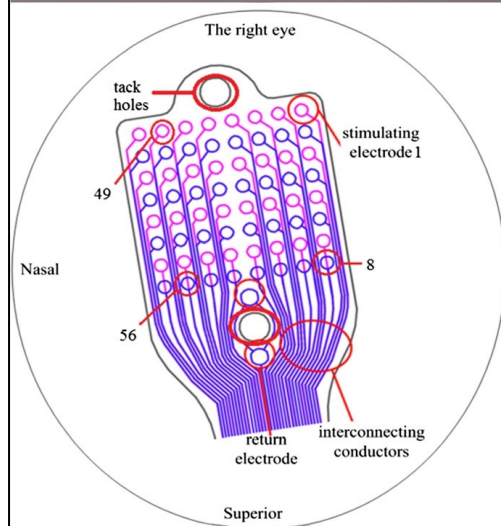
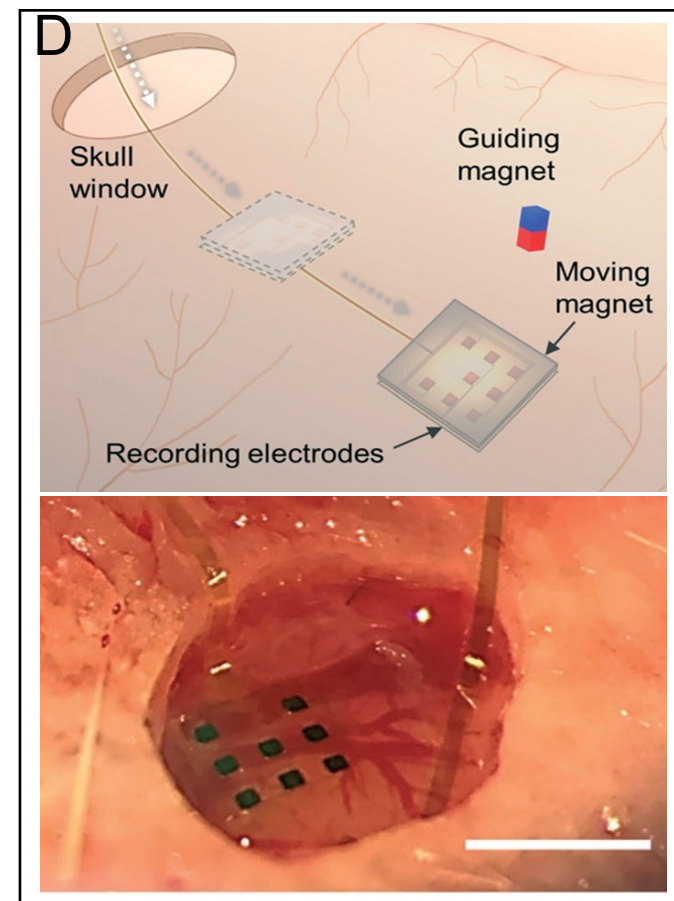
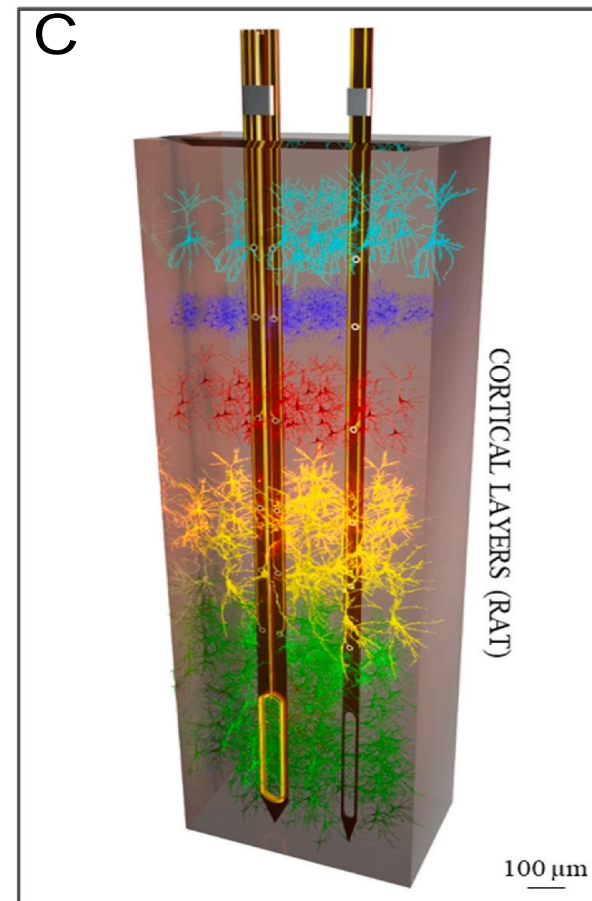
CC BY-NC

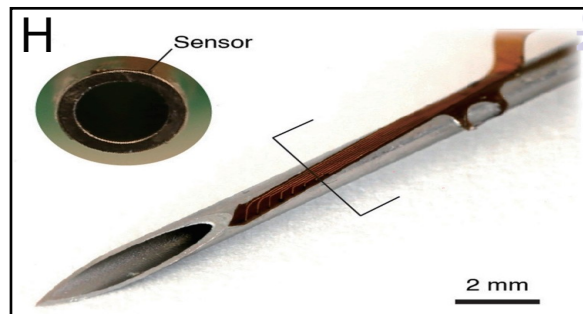
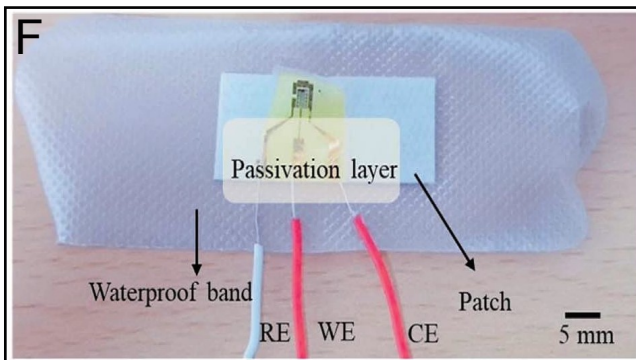
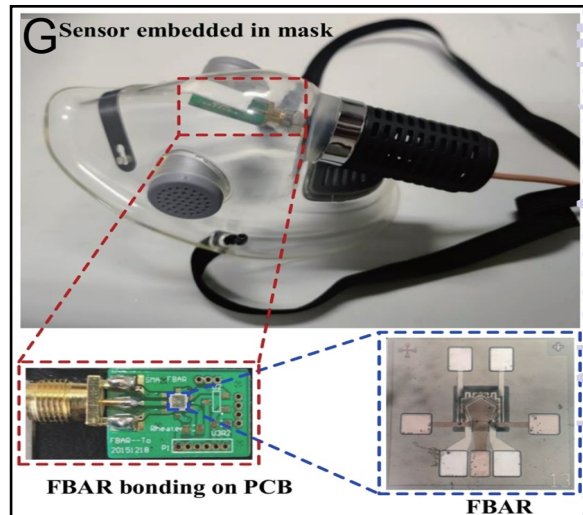
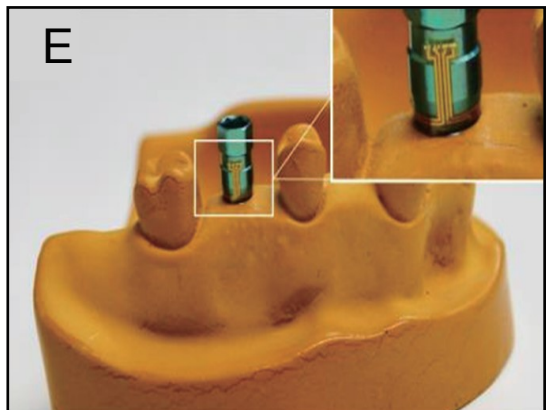
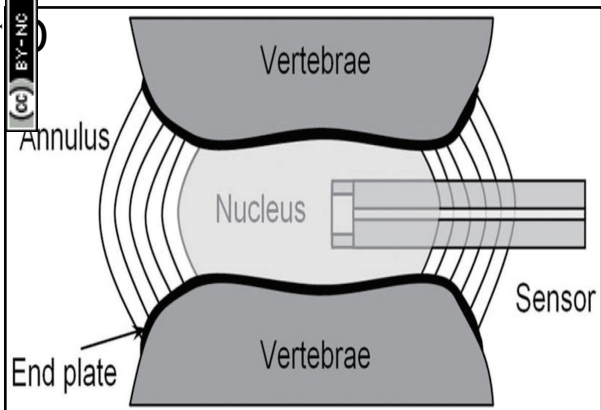
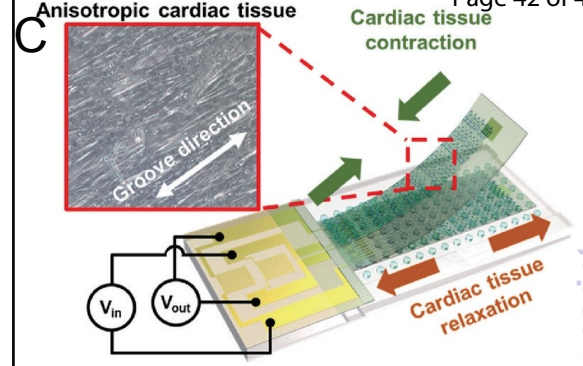
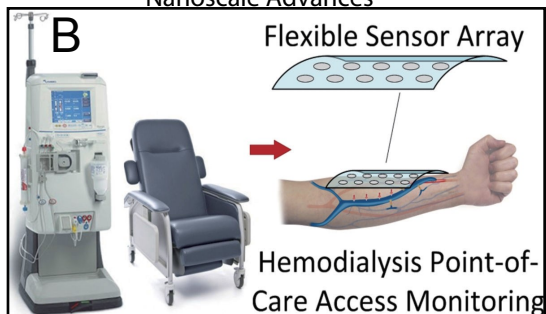
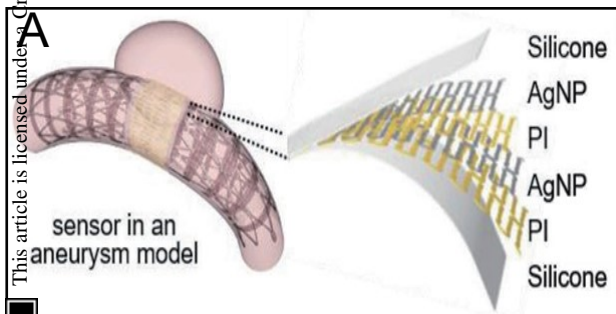
Thin film electrode

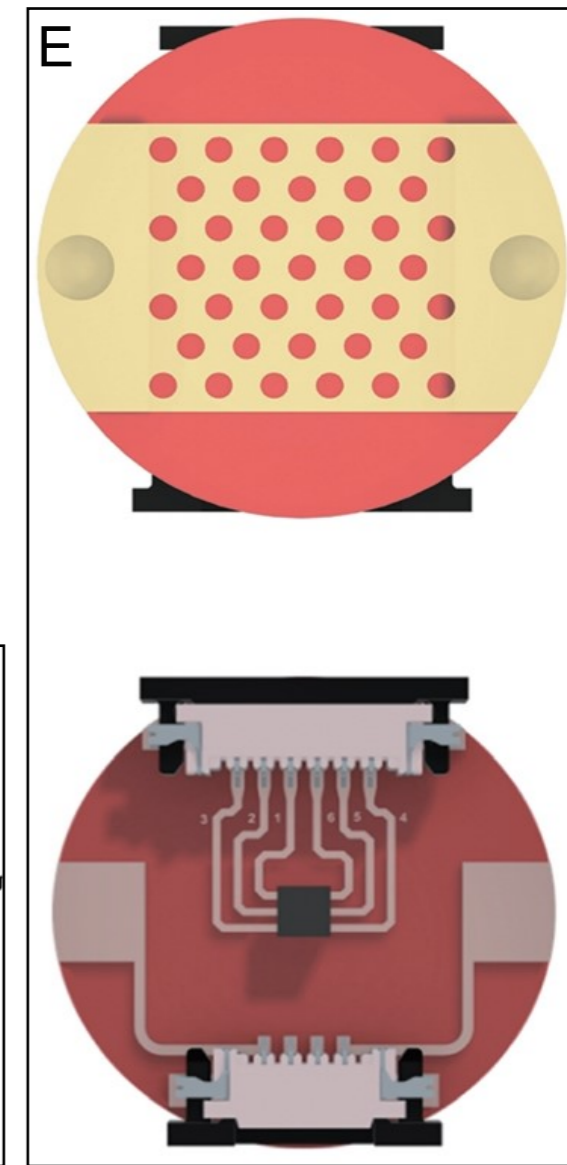
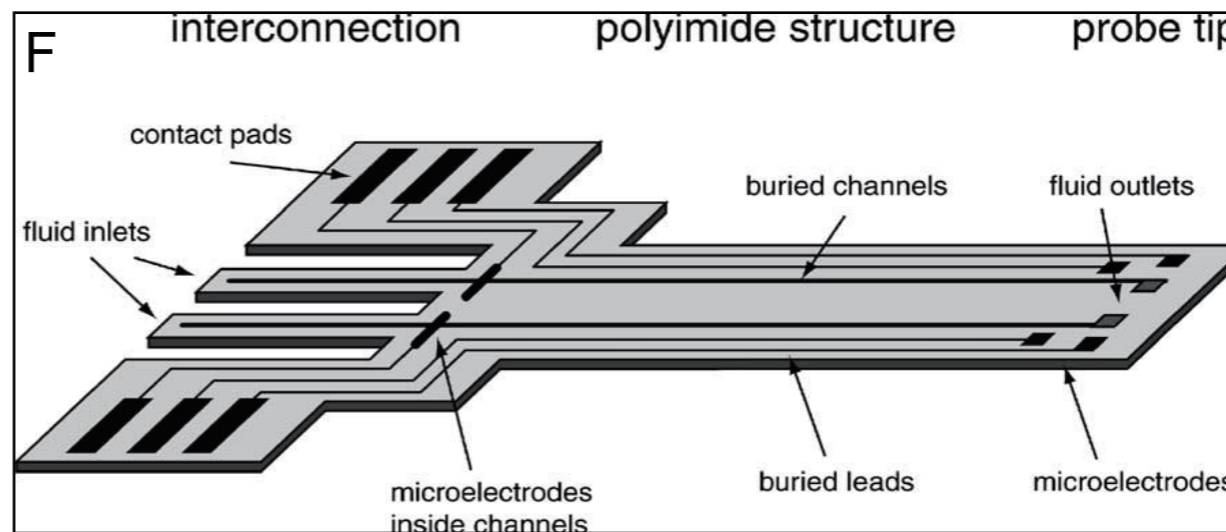
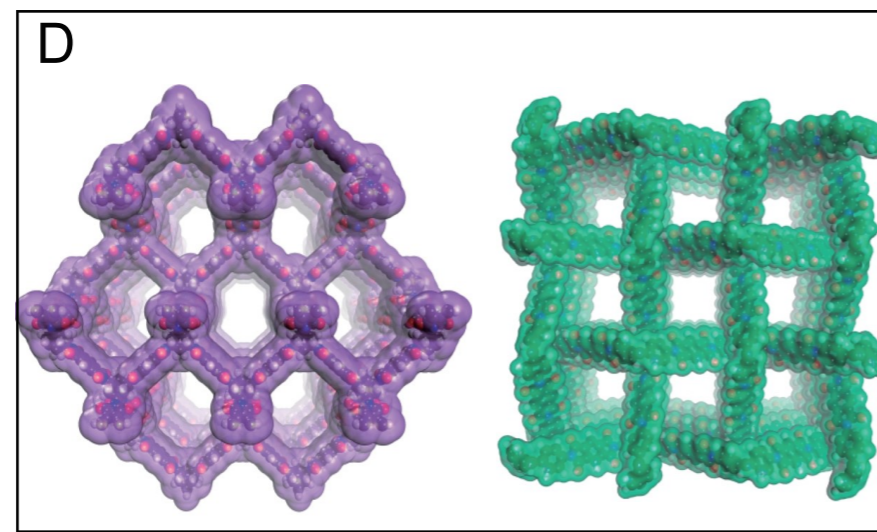
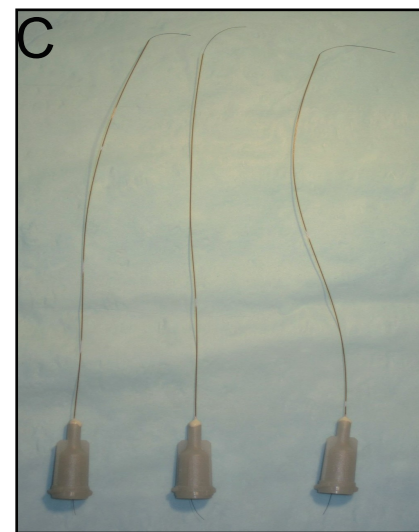
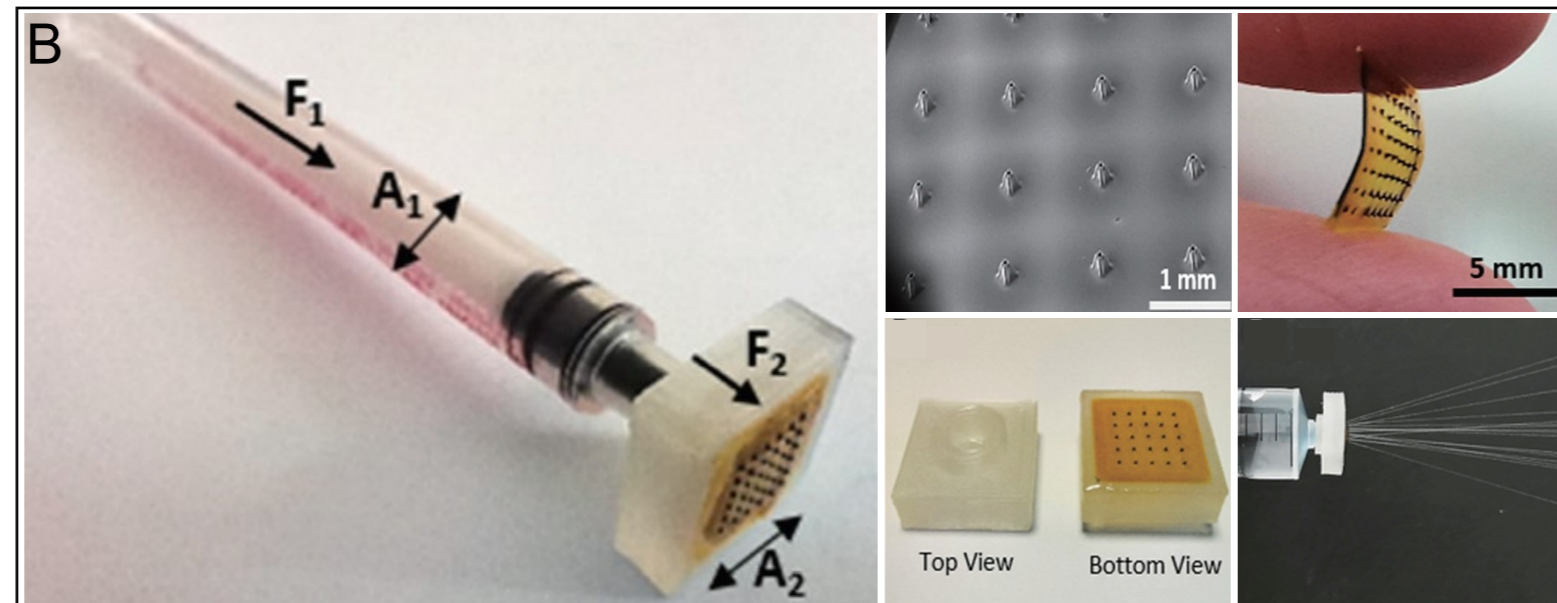
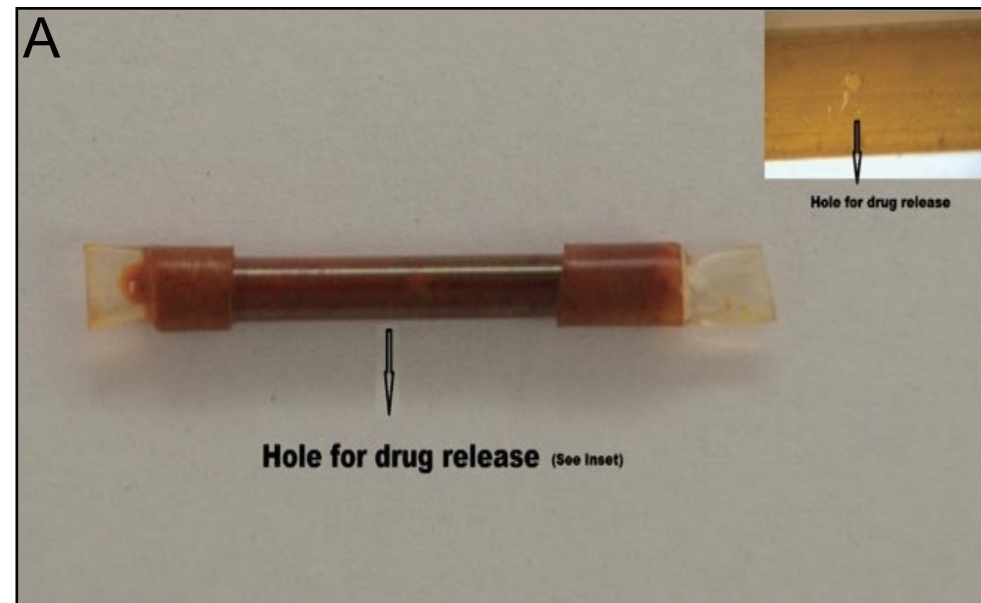


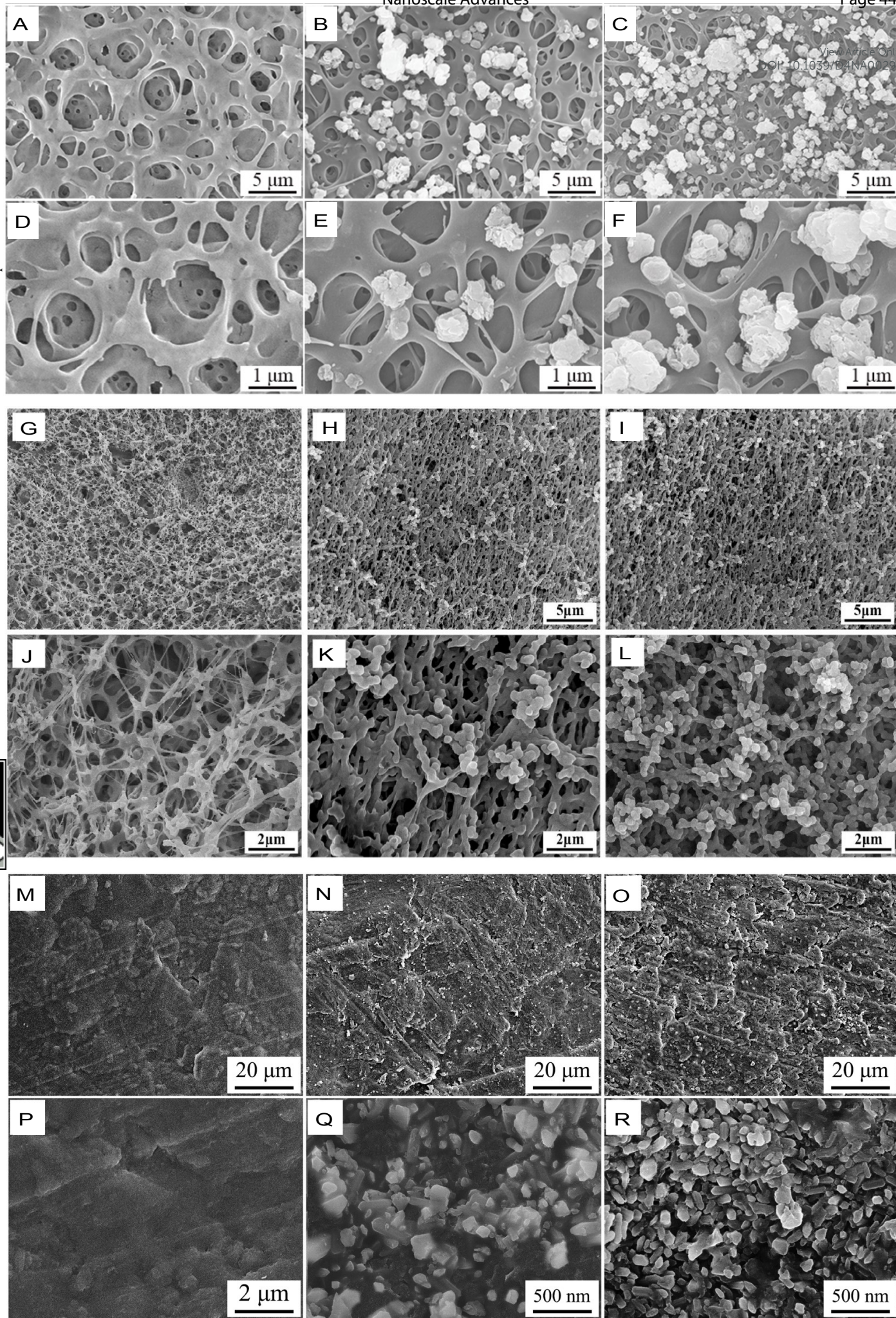


Nanoscale Advances









View Article Online  
DOI: 10.1039/B4NA00292J

Open Access Article. Published on 04 2024. Downloaded on 10-07-2024 12:30:10.  
This article is licensed under a Creative Commons Attribution-NonCommercial 3.0 Unported Licence.



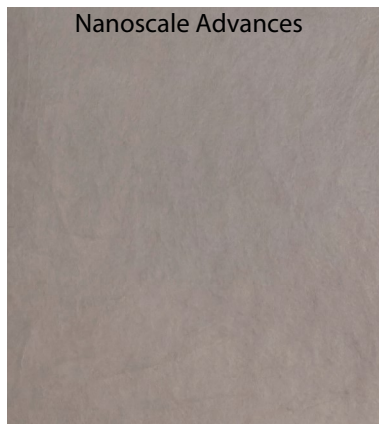
Nanoscale Advances Accepted Manuscript



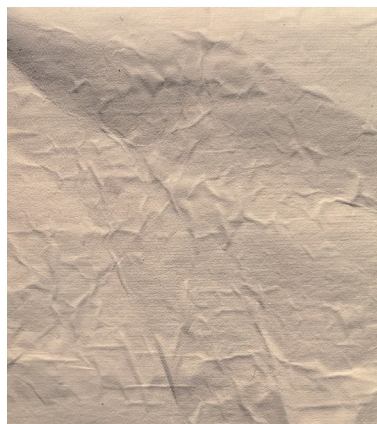
PI film 1



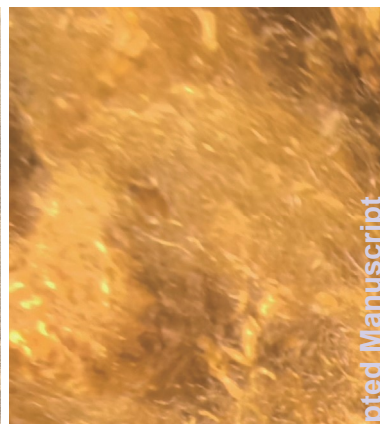
PI film 2



PI film 3



PI patch



PI fiber



PI fabrics 1



PI fabrics 2



PI fabrics 3



PI fabrics 4



PI gauze